SIAM J. SCI. COMPUT.
Vol. 31, No. 3, pp. 1742–1773

CENTRAL-UPWIND SCHEMES FOR TWO-LAYER SHALLOW WATER EQUATIONS*

ALEXANDER KURGANOV† AND GUERGANA PETROVA‡

Abstract. We derive a second-order semidiscrete central-upwind scheme for one- and two-dimensional systems of two-layer shallow water equations. We prove that the presented scheme is well-balanced in the sense that stationary steady-state solutions are exactly preserved by the scheme and positivity preserving; that is, the depth of each fluid layer is guaranteed to be nonnegative. We also propose a new technique for the treatment of the nonconservative products describing the momentum exchange between the layers. The performance of the proposed method is illustrated on a number of numerical examples, in which we successfully capture (quasi) steady-state solutions and propagating interfaces.

Key words. hyperbolic systems of conservation and balance laws, semidiscrete central-upwind schemes, nonconservative products, two-layer shallow water equations

AMS subject classifications. 76M12, 35L65, 76T99

DOI. 10.1137/080719091

1. Introduction.

We develop a Godunov-type central-upwind scheme for the system of two-layer shallow water equations. This system is obtained from the compressible isentropic Euler equations by vertical averaging across each layer depth. The layers are assumed to have different constant densities $\rho_1 < \rho_2$ due to, for example, different water salinity, and to be immiscible. The studied one- and two-dimensional two-layer shallow water systems are extensions of the Saint-Venant systems [11], which are widely used in both geophysical science and coast and dams-keeping engineering.

The one-dimensional (1-D) two-layer shallow water model describes a flow that consists of two layers of heights h_1 (upper layer) and h_2 (lower layer) at position x at time t with corresponding velocities u_i and discharges $q_i := h_i u_i$, $i = 1, 2$. The two-layer system we consider is the model studied in [5], which describes a flow in a straight channel with a bottom topography B. It is given by

$$\begin{cases} (h_1)_t + (q_1)_x = 0, \\ (q_1)_t + \left(h_1 u_1^2 + \frac{g}{2} h_1^2\right)_x = -g h_1 B_x - g h_1 (h_2)_x, \\ (h_2)_t + (q_2)_x = 0, \\ (q_2)_t + \left(h_2 u_2^2 + \frac{g}{2} h_2^2\right)_x = -g h_2 B_x - g h_2 \left(\widehat{h}_1\right)_x, \end{cases} \tag{1.1}$$

where g is the gravitational constant, $r := \frac{\rho_1}{\rho_2}$ is the constant density ratio, and $\widehat{h}_1 := r h_1$.

The 2-D generalization of (1.1) is (for details see, e.g., [28]) the following system

*Received by the editors March 22, 2008; accepted for publication (in revised form) November 10, 2008; published electronically February 27, 2009.

http://www.siam.org/journals/sisc/31-3/71909.html

†Mathematics Department, Tulane University, New Orleans, LA 70118 (kurganov@math.tulane.edu). The work of this author was supported in part by NSF grant DMS-0610430.

‡Department of Mathematics, Texas A & M University, College Station, TX 77843 (gpetrova@math.tamu.edu). The work of this author was supported in part by NSF grants DMS-0505501 and DMS-0810869 and by award KUS-C1-016-04 made by King Abdullah University of Science and Technology (KAUST).

of equations:

$$
\begin{cases}
(h_1)_t + (q_1)_x + (p_1)_y = 0,\\
(q_1)_t + \left[h_1u_1^2 + \frac{g}{2}(h_1+h_2+B)(h_1-h_2-B)\right]_x + (h_1u_1v_1)_y\\
\qquad\qquad = -g(h_1+h_2+B)(B+h_2)_x,\\
(p_1)_t + (h_1u_1v_1)_x + \left[h_1v_1^2 + \frac{g}{2}(h_1+h_2+B)(h_1-h_2-B)\right]_y\\
\qquad\qquad = -g(h_1+h_2+B)(B+h_2)_y,\\
(h_2)_t + (q_2)_x + (p_2)_y = 0,\\
(q_2)_t + \left[h_2u_2^2 + \frac{g}{2}\left(h_2+\widehat{h}_1+B\right)\left(h_2-\widehat{h}_1-B\right)\right]_x + (h_2u_2v_2)_y\\
\qquad\qquad = -g\left(h_2+\widehat{h}_1+B\right)\left(B+\widehat{h}_1\right)_x,\\
(p_2)_t + (h_2u_2v_2)_x + \left[h_2v_2^2 + \frac{g}{2}\left(h_2+\widehat{h}_1+B\right)\left(h_2-\widehat{h}_1-B\right)\right]_y\\
\qquad\qquad = -g\left(h_2+\widehat{h}_1+B\right)\left(B+\widehat{h}_1\right)_y,
\end{cases}
\tag{1.2}
$$

where the y-velocities and discharges are denoted by v_i and $p_i := h_iv_i$, $i = 1, 2$, respectively, and the rest of the notation is the same as in the 1-D case.

Other multilayer shallow water models are also available. For example, we refer the reader to [2], where a new approximation of the Navier–Stokes equations consisting of a set of coupled Saint-Venant systems is proposed.

In this paper, we numerically study the systems (1.1) and (1.2). Computing their solutions is a challenging problem due to several reasons: they contain nonconservative product terms, they are only conditionally hyperbolic, and their eigenstructure cannot be obtained in explicit form. Even though these factors make it quite difficult to design upwind methods for the two-layer shallow water equations, several upwind-based schemes, including the finite-volume [5, 6, 12] and finite-element [28] ones, were developed during the past decade. An interesting approach to overcome the above difficulties has been recently proposed in [1], where two artificial equations have been added to the system (1.1) so that the extended system becomes hyperbolic and, thus, could be solved by a second-order Roe-type scheme in a rather straightforward manner. A time-splitting approach, proposed in [4], is another way to implement upwinding without having the full eigenstructure of the system readily available.

Some of the above methods [1, 4, 5, 6, 12] are well-balanced in the sense that they exactly preserve stationary steady-state solutions given by

$$u_1 \equiv v_1 \equiv u_2 \equiv v_2 \equiv 0, \quad h_1 \equiv \text{const}, \quad w := h_2 + B \equiv \text{const}.$$

However, only one of them, the time-splitting method [4], is also positivity preserving; that is, it guarantees that the computed values of $h_i \geq 0$, $i = 1, 2$, for all times. Note that even though the time-splitting method in [4] is well-balanced and positivity preserving it lacks conservation of the total momentum, which may lead to the appearance of unphysical solutions; see the numerical examples reported in [4]. Both properties—well-balancedness and positivity preserving—are absolutely necessary for the design of a numerical scheme for the two-layer shallow water system since they guarantee the stability of the method. Here, we propose a second-order semidiscrete central-upwind scheme that satisfies both properties.

An additional challenge in the development of reliable and robust numerical methods for two-layer shallow water systems is the discretization of the nonconser-

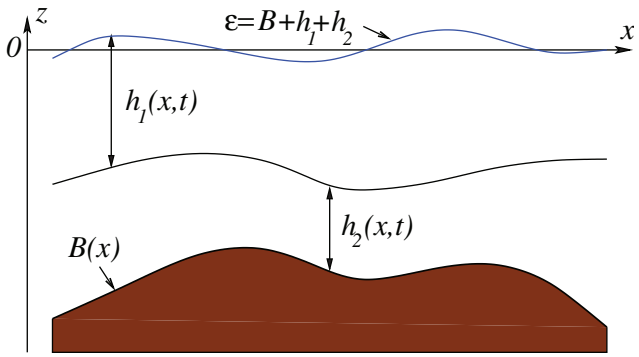

FIG. 1.1. *Two-layer shallow water setup.*

vative products appearing on the right-hand side (RHS) of (1.1) and (1.2). Similar terms arise in many different multicomponent models since moment/energy exchange terms are typically expressed in terms of nonconservative products. Their presence makes the analysis of the corresponding PDEs extremely challenging (see, e.g., [3, 7, 8, 9, 10, 25]), and a rigorous mathematical theory of such systems has not been completely developed yet. At the same time, practical applications require us to design numerical methods capable of treating nonconservative terms in a consistent and stable manner. One may attempt to use a global upwinding approach (see, e.g., [1, 4, 5]) or to discretize these terms in a way that ensures the well-balanced property of the resulting scheme (see, e.g., [12]), or to simply discretize these terms directly. However, different nonconservative term discretizations may lead to qualitatively different computed solutions, which makes it impossible to design a reliable robust numerical method.

Here, we propose a new way to practically solve this problem. We simply rewrite the two-layer shallow water systems in an equivalent (for smooth solutions) form, suitable for a "favorable" treatment of the nonconservative products. Our approach uses the fact that, in the relevant applications, fluctuations of the total water level $\varepsilon := h_1+h_2+B$ are relatively small, that is, after choosing a proper coordinate system $\varepsilon \sim 0$ (see Figure 1.1). Thus, we reduce as much as possible the "influence" of the particular choice of the nonconservative products discretization by rewriting the systems (1.1) and (1.2) so that the nonconservative product terms become proportional to ε. The rewritten systems are then numerically solved by a two-layer version of the second-order well-balanced positivity preserving central-upwind scheme, recently developed in [22] for the original (single-layer) Saint-Venant systems.

Central-upwind schemes, first introduced in [23] and further developed in [20, 21, 24], belong to the class of Riemann-problem-solver free Godunov-type central schemes. Their increasing popularity for solving various practical problems is due to the fact that they can be used as a "black-box solver" that uses only partial information of the system eigenstructure, namely, the upper/lower bounds on the largest/smallest eigenvalues of the Jacobian of the flux. Therefore, the extension of the central-upwind schemes from the single- to two-layer case is quite straightforward even though the two-layer system is substantially more complicated than the single-layer one.

As in the single-layer case, the positivity of the depth of each fluid layer is guaranteed by the use of a special positivity preserving piecewise linear reconstruction of the computed solution. The well-balanced property is achieved with the help of a

special discretization of the geometric source term appearing in (1.1) and (1.2) due to a nonflat bottom topography. These two properties, well-balancedness and positivity preserving, are essential for accurately capturing quasi-steady states and states in which $h_1 \approx 0$ and/or $h_2 \approx 0$.

The paper is organized as follows. In section 2, we first rewrite the 1-D system (1.1) in a computationally friendly form and describe the central-upwind scheme for the modified system. The description includes a special discretization of the bottom topography function B (section 2.1) the nonconservative products (section 2.4), and a well-balanced discretization of the geometric source term (section 2.5). A positivity preserving piecewise linear reconstruction is described in section 2.3. We then prove the well-balanced and positivity preserving properties of the proposed scheme (section 2.6) and test it on several numerical examples (section 2.7). The same issues, but for the 2-D system (1.2), are addressed in section 3.

2. One-dimensional scheme. We first rewrite the system (1.1) in a different form in terms of the new variables $\mathbf{U} := (h_1, q_1, w, q_2)^T$, where $w := h_2 + B$ and, thus, $\varepsilon = h_1 + w$:

$$
\begin{cases}
(h_1)_t + (q_1)_x = 0, \\
(q_1)_t + \left(\dfrac{q_1^2}{h_1} + g\varepsilon h_1 \right)_x = g\varepsilon (h_1)_x, \\
w_t + (q_2)_x = 0, \\
(q_2)_t + \left(\dfrac{q_2^2}{w - B} + \dfrac{g}{2} w^2 - \dfrac{g}{2} r h_1^2 - gB\widehat{\varepsilon} \right)_x = -g\widehat{\varepsilon} B_x - g\varepsilon \left(\widehat{h}_1 \right)_x,
\end{cases}
\tag{2.1}
$$

where $\widehat{\varepsilon} := \widehat{h}_1 + w$. For smooth solutions, this system is equivalent to the original 1-D system (1.1). No rigorous mathematical theory of weak solutions is available for either (1.1) or (2.1), but the new system (2.1) is preferable for numerical computations thanks to the following two reasons:

(i) The stationary steady state for (1.1) is given by $\mathbf{U} \equiv (C_1, 0, C_2, 0)^T$, with C_1, C_2 constants. Thus, the new formulation (2.1) simplifies the process of designing a well-balanced scheme for the two-layer shallow water equations.

(ii) The coefficients in the nonconservative products $g\varepsilon(h_1)_x$ and $g\varepsilon(\widehat{h}_1)_x$ in (2.1) are proportional to ε, which vanishes at stationary steady states, and, what is even more important, in most oceanographic applications remains very small. This situation is illustrated by the surface waves in the ocean: their amplitude is always much smaller than the total depth of the water layers $h_1 + h_2$. As it is clearly indicated by our numerous numerical experiments, smallness of ε makes the computed solution practically independent of the way the nonconservative terms in (2.1) are discretized. We note that when $r \sim 1$ the variable $\widehat{\varepsilon}$ is also expected to be small in typical oceanographic applications.

We numerically solve the system (2.1) by a modified version of the well-balanced positivity preserving central-upwind scheme from [22], developed for the single-layer shallow water equations. We begin with introducing a uniform grid (an extension to a nonuniform grid is straightforward) $x_\alpha := \alpha \Delta x$, where Δx is a small spatial scale, and denoting by I_j the finite volume cells $I_j := [x_{j-\frac{1}{2}}, x_{j+\frac{1}{2}}]$.

As in the single-layer case [22], the well-balanced and positivity preserving property of the scheme relies on a special discretization of the bottom topography function B, which is described below.

2.1. Bottom discretization. Following [22], we replace the bottom topography function B with its continuous piecewise linear approximation $\widetilde{B}$, consisting of the linear pieces that connect the points $(x_{j-\frac12}, B_{j-\frac12})$ and $(x_{j+\frac12}, B_{j+\frac12})$:

$$\widetilde{B}(x) = B_{j-\frac12} + \left(B_{j+\frac12} - B_{j-\frac12}\right)\cdot\frac{x - x_{j-\frac12}}{\Delta x}, \quad x_{j-\frac12} \le x \le x_{j+\frac12}, \tag{2.2}$$

where

$$B_{j+\frac12} := \frac{B(x_{j+\frac12}+0) + B(x_{j+\frac12}-0)}{2}, \tag{2.3}$$

which reduces to $B_{j+\frac12} = B(x_{j+\frac12})$ if B is continuous at $x = x_{j+\frac12}$.

Replacing B with $\widetilde{B}$ does not affect the (formal) order of the central-upwind scheme since the piecewise linear interpolant (2.2) is a (formally) second-order approximation of B. The reason for introducing $\widetilde{B}$ is that, unlike the original bottom topography function, it satisfies the following two properties. First, its point values at the cell centers $x = x_j$ coincide with its cell averages over the corresponding cells; second, these values are also equal to the average of the values of $\widetilde{B}$ at the end points of I_j, namely,

$$B_j := \widetilde{B}(x_j) = \frac{1}{\Delta x}\int_{I_j}\widetilde{B}(x)\,dx = \frac{B_{j+\frac12} + B_{j-\frac12}}{2}. \tag{2.4}$$

Equation (2.4) is important for the analysis of the new scheme and plays an essential role in the proof of the positivity preserving property of the scheme (see Theorem 2.1). Notice that if one takes B_j to be the value of the bottom topography function at $x = x_j$, that is, if one sets $B_j = B(x_j)$, as it was done in [19], (2.4) would not hold.

2.2. Semidiscrete central-upwind scheme. Let us first introduce notations for the flux $\mathbf{F}$, the geometric source term $\mathbf{S}$, and the nonconservative products $\mathbf{N}$ of the system (2.1):

$$\begin{aligned}&\mathbf{F}(\mathbf{U},B) := \left(q_1, \frac{q_1^2}{h_1} + g\varepsilon h_1, q_2, \frac{q_2^2}{w-B} + \frac{g}{2}w^2 - \frac{g}{2}rh_1^2 - gB\widehat{\varepsilon}\right)^T,\\ &\mathbf{S}(\mathbf{U},B) := (0,0,0,-g\widehat{\varepsilon}B_x)^T, \quad \mathbf{N}(\mathbf{U},B) := \left(0, g\varepsilon(h_1)_x, 0, -g\varepsilon\left(\widehat{h}_1\right)_x\right)^T.\end{aligned} \tag{2.5}$$

Using these notations, a semidiscretization of (2.1) can be written as the following system of ODEs:

$$\frac{d}{dt}\overline{\mathbf{U}}_j(t) = -\frac{\mathbf{H}_{j+\frac12}(t) - \mathbf{H}_{j-\frac12}(t)}{\Delta x} + \overline{\mathbf{S}}_j(t) + \overline{\mathbf{N}}_j(t), \tag{2.6}$$

where $\overline{\mathbf{U}}_j(t)$ are approximations of the cell averages of the solution over the corresponding cells

$$\overline{\mathbf{U}}_j(t) \approx \frac{1}{\Delta x}\int_{I_j}\mathbf{U}(x,t)\,dx, \quad \mathbf{U} := (h_1, q_1, w, q_2)^T,$$

$\mathbf{H}_{j+\frac12}$ are numerical fluxes, and $\overline{\mathbf{S}}_j$ and $\overline{\mathbf{N}}_j$ are discretizations of the cell averages of the source and nonconservative product terms, respectively:

$$\overline{\mathbf{S}}_j(t) \approx \frac{1}{\Delta x}\int_{I_j}\mathbf{S}(\mathbf{U}(x,t),B(x))\,dx, \quad \overline{\mathbf{N}}_j(t) \approx \frac{1}{\Delta x}\int_{I_j}\mathbf{N}(\mathbf{U}(x,t),B(x))\,dx.$$

The central-upwind numerical fluxes $\mathbf{H}_{j+\frac{1}{2}}$ are the ones proposed in [21] (see also [13, 17]), namely,

$$\begin{aligned}\mathbf{H}_{j+\frac{1}{2}}(t) &= \frac{a^+_{j+\frac{1}{2}}\mathbf{F}\left(\mathbf{U}^-_{j+\frac{1}{2}}, B_{j+\frac{1}{2}}\right) - a^-_{j+\frac{1}{2}}\mathbf{F}\left(\mathbf{U}^+_{j+\frac{1}{2}}, B_{j+\frac{1}{2}}\right)}{a^+_{j+\frac{1}{2}} - a^-_{j+\frac{1}{2}}}\\ &\quad + \frac{a^+_{j+\frac{1}{2}}a^-_{j+\frac{1}{2}}}{a^+_{j+\frac{1}{2}} - a^-_{j+\frac{1}{2}}}\left[\mathbf{U}^+_{j+\frac{1}{2}} - \mathbf{U}^-_{j+\frac{1}{2}}\right],\end{aligned} \tag{2.7}$$

where $B_{j+\frac{1}{2}}$ are defined in (2.3). The values $\mathbf{U}^{\pm}_{j+\frac{1}{2}}$ are the right/left point values at $x = x_{j+\frac{1}{2}}$ of the conservative piecewise linear reconstruction $\widetilde{\mathbf{U}}$,

$$\widetilde{\mathbf{U}}(x) := \overline{\mathbf{U}}_j + (\mathbf{U}_x)_j(x - x_j), \quad x_{j-\frac{1}{2}} < x < x_{j+\frac{1}{2}}, \tag{2.8}$$

which is used to approximate $\mathbf{U}$ at time t, that is,

$$\mathbf{U}^{\pm}_{j+\frac{1}{2}} := \widetilde{\mathbf{U}}\left(x_{j+\frac{1}{2}} \pm 0\right) = \overline{\mathbf{U}}_{j+\frac{1}{2}\pm\frac{1}{2}} \mp \frac{\Delta x}{2}(\mathbf{U}_x)_{j+\frac{1}{2}\pm\frac{1}{2}}. \tag{2.9}$$

Here, the numerical derivatives $(\mathbf{U}_x)_j$ are (at least) first-order, componentwise approximations of $\mathbf{U}_x(x_j, t)$, computed using a nonlinear limiter needed to ensure the nonoscillatory nature of the reconstruction (2.8). The right- and left-sided local speeds $a^{\pm}_{j+\frac{1}{2}}$ in (2.7) are obtained from the largest and the smallest eigenvalues of the Jacobian $\frac{\partial \mathbf{F}}{\partial \mathbf{U}}$ (see section 2.3 for details). Note that the quantities $\overline{\mathbf{U}}_j$, $\mathbf{U}^{\pm}_{j+\frac{1}{2}}$, $(\mathbf{U}_x)_j$, and $a^{\pm}_{j+\frac{1}{2}}$ in (2.7) depend on t, but we simplify the notation by suppressing this dependence.

Finally, a fully discrete central-upwind scheme is obtained by applying an appropriate ODE solver to (2.6). In our numerical experiments, we have used the third-order strong stability preserving Runge–Kutta (SSP-RK) method from [16, 33, 34].

2.3. Positivity preserving piecewise linear reconstruction. In this section, we discuss the details of the evaluation of the numerical derivatives $(\mathbf{U}_x)_j$ used in the piecewise linear reconstruction (2.8). This is a crucial step in the construction of our method since the nonoscillatory property and nonlinear stability of the resulting scheme hinges on the nonoscillatory property of the reconstruction, which is typically achieved when the numerical derivatives are computed using a nonlinear limiter. A library of reliable limiters is available (see, e.g., [15, 18, 26, 27, 30, 35, 36]), and the proposed central-upwind scheme can be implemented with any of the limiters described in the above references. In the numerical experiments reported below, we have used the generalized minmod limiter [27, 30, 35]:

$$(\mathbf{U}_x)_j = \text{minmod}\left(\theta\frac{\overline{\mathbf{U}}_j - \overline{\mathbf{U}}_{j-1}}{\Delta x}, \frac{\overline{\mathbf{U}}_{j+1} - \overline{\mathbf{U}}_{j-1}}{2\Delta x}, \theta\frac{\overline{\mathbf{U}}_{j+1} - \overline{\mathbf{U}}_j}{\Delta x}\right), \quad \theta \in [1, 2], \tag{2.10}$$

where the minmod function is defined as

$$\text{minmod}(z_1, z_2, \ldots) := \begin{cases}\min_j\{z_j\} & \text{if } z_j > 0 \ \forall j,\\ \max_j\{z_j\} & \text{if } z_j < 0 \ \forall j,\\ 0 & \text{otherwise}\end{cases} \tag{2.11}$$

and the parameter θ can be used to control the amount of numerical viscosity present in the resulting scheme: larger values of θ correspond to less dissipative but, in general, more oscillatory reconstructions.

Unfortunately, the use of a nonlinear limiter by itself cannot guarantee positivity of the reconstructed point values $(h_1)^{\pm}_{j+\frac12}$ and $(h_2)^{\pm}_{j+\frac12}$, even when the cell averages $(\overline{h}_1)_j$ and $(\overline{h}_2)_j$ are positive for all j. The positivity of $(h_1)^{\pm}_{j+\frac12}$ is relatively easy to ensure: one has to use a positivity preserving reconstruction for h_1. For example, the generalized minmod reconstruction satisfies this requirement since the reconstructed point values $(h_1)^{\pm}_{j+\frac12}$ are always between the neighboring cell averages $(\overline{h}_1)_j$ and $(\overline{h}_1)_{j+1}$. However, the same approach would not guarantee positivity of $(h_2)^{\pm}_{j+\frac12}$ since these point values are obtained from the reconstructed values of $w^{\pm}_{j+\frac12}$ by

$$(h_2)^{\pm}_{j+\frac12} := w^{\pm}_{j+\frac12} - B_{j+\frac12}, \tag{2.12}$$

and, thus, it could happen that $(h_2)^{\pm}_{j+\frac12} < 0$. This can be illustrated even by the simplest first-order piecewise constant reconstruction, obtained by setting the slopes $(w_x)_j = 0$ for all j. In this case, the reconstructed point values of h_2 may be negative since the cell average values $\overline{w}_j$ and $\overline{w}_{j+1}$ may be smaller than $B_{j+\frac12}$. Therefore, we have to correct the original nonoscillatory reconstruction for the w component in (2.8) to ensure that the computed in (2.12) values $(h_2)^{\pm}_{j+\frac12} \geq 0\ \forall j$, provided $(\overline{h}_2)_j := \overline{w}_j - B_j \geq 0\ \forall j$. In fact, we need to correct the reconstruction for $\widetilde{w}$ only in the following two cases:

$$\text{if } \ w^{-}_{j+\frac12} < B_{j+\frac12}, \ \text{ then take } \ (w_x)_j := \frac{B_{j+\frac12} - \overline{w}_j}{\frac{\Delta x}{2}},$$

$$\Longrightarrow \ w^{-}_{j+\frac12} = B_{j+\frac12}, \ \ w^{+}_{j-\frac12} = 2\overline{w}_j - B_{j+\frac12}; \tag{2.13}$$

$$\text{if } \ w^{+}_{j-\frac12} < B_{j-\frac12}, \ \text{ then take } \ (w_x)_j := \frac{\overline{w}_j - B_{j-\frac12}}{\frac{\Delta x}{2}},$$

$$\Longrightarrow \ w^{-}_{j+\frac12} = 2\overline{w}_j - B_{j-\frac12}, \ \ w^{+}_{j-\frac12} = B_{j-\frac12}. \tag{2.14}$$

We note that the same correction procedure has been applied in a single-layer case in [22] to ensure the positivity of the reconstructed water depth values.

It is obvious that this correction procedure guarantees that the resulting reconstruction $\widetilde{w}$ will remain conservative and its graph will be above the piecewise linear approximant of the bottom topography function $\widetilde{B}$. Therefore, the corrected values of $(h_2)^{\pm}_{j+\frac12}$, subsequently, computed from (2.12) will be nonnegative (this feature of the modified reconstruction is used in section 2.6, where we prove the positivity preserving property of our new central-upwind scheme).

Notice, however, that even though our reconstruction-correction procedure guarantees that the values $(h_i)^{\pm}_{j+\frac12}$, $i = 1, 2$, will be nonnegative, they may be very small or even zero. This will not allow us to (accurately) compute the quantities $(q_i)^{\pm}_{j+\frac12}/(h_i)^{\pm}_{j+\frac12}$, $i = 1, 2$, required for the computation of the numerical flux. We avoid the division by very small numbers in the computation of the velocities using the following formula, suggested in [22] (for simplicity, we omit the $\pm$ and $j \pm \frac12$ indexes):

$$u_i = \frac{\sqrt{2}\, h_i\, q_i}{\sqrt{(h_i)^4 + \max((h_i)^4, \delta)}}, \quad i = 1, 2, \tag{2.15}$$

where δ is a small a priori chosen positive number (in all of our numerical experiments, $\delta = (\Delta x)^4$). As one can easily see, this formula reduces to $u_i = q_i/h_i$ for large values of

h_i, but when h_i is small the entire algorithm remains consistent only if we recompute q_i using

$$q_i := h_i \cdot u_i, \quad i = 1, 2, \tag{2.16}$$

where u_i are computed by (2.15). We emphasize that if the originally reconstructed q_i are not replaced by $h_i \cdot u_i$, then the proof of Theorem 2.1 fails and, moreover, the scheme may produce negative values of h_i as confirmed by our numerical experiments.

Finally, equipped with the values of $(h_i)^{\pm}_{j+\frac{1}{2}}$ and $(u_i)^{\pm}_{j+\frac{1}{2}}$, $i = 1, 2$, we compute the one-sided local speeds of propagation (see, e.g., [21, 24]):

$$\begin{aligned} a^{+}_{j+\frac{1}{2}} &= \max_{\pm}\Big\{\big(\lambda^{\pm}_1\big)_{j+\frac{1}{2}}, \big(\lambda^{\pm}_2\big)_{j+\frac{1}{2}}, \big(\lambda^{\pm}_3\big)_{j+\frac{1}{2}}, \big(\lambda^{\pm}_4\big)_{j+\frac{1}{2}}, 0\Big\},\\ a^{-}_{j+\frac{1}{2}} &= \min_{\pm}\Big\{\big(\lambda^{\pm}_1\big)_{j+\frac{1}{2}}, \big(\lambda^{\pm}_2\big)_{j+\frac{1}{2}}, \big(\lambda^{\pm}_3\big)_{j+\frac{1}{2}}, \big(\lambda^{\pm}_4\big)_{j+\frac{1}{2}}, 0\Big\}, \end{aligned} \tag{2.17}$$

where $\lambda^{\pm}_i := \lambda_i(h^{\pm}_1, u^{\pm}_1, h^{\pm}_2, u^{\pm}_2)$ are the eigenvalues of the Jacobian $\frac{\partial \mathbf{F}}{\partial \mathbf{U}}$. Here, in order to guarantee the positivity preserving property of the scheme (see Theorem 2.1), we impose an additional requirement on the local speeds: they should be bounded by $(u_1)^{\pm}_{j+\frac{1}{2}}$ and $(u_2)^{\pm}_{j+\frac{1}{2}}$; namely, we replace (2.17) with

$$\begin{aligned} a^{+}_{j+\frac{1}{2}} &= \max_{\pm}\Big\{\big(\lambda^{\pm}_1\big)_{j+\frac{1}{2}}, \big(\lambda^{\pm}_2\big)_{j+\frac{1}{2}}, \big(\lambda^{\pm}_3\big)_{j+\frac{1}{2}}, \big(\lambda^{\pm}_4\big)_{j+\frac{1}{2}}, (u_1)^{\pm}_{j+\frac{1}{2}}, (u_2)^{\pm}_{j+\frac{1}{2}}, 0\Big\},\\ a^{-}_{j+\frac{1}{2}} &= \min_{\pm}\Big\{\big(\lambda^{\pm}_1\big)_{j+\frac{1}{2}}, \big(\lambda^{\pm}_2\big)_{j+\frac{1}{2}}, \big(\lambda^{\pm}_3\big)_{j+\frac{1}{2}}, \big(\lambda^{\pm}_4\big)_{j+\frac{1}{2}}, (u_1)^{\pm}_{j+\frac{1}{2}}, (u_2)^{\pm}_{j+\frac{1}{2}}, 0\Big\}. \end{aligned} \tag{2.18}$$

The eigenvalues $\lambda_1, \dots, \lambda_4$ of the Jacobian $\frac{\partial \mathbf{F}}{\partial \mathbf{U}}$ are to be determined from the characteristic equation (see [5])

$$\big(\lambda^2 - 2u_1\lambda + u_1^2 - gh_1\big)\big(\lambda^2 - 2u_2\lambda + u_2^2 - gh_2\big) = g^2\widehat{h}_1 h_2. \tag{2.19}$$

We are mainly interested in the case when $r \sim 1$ and $u_1 \sim u_2$, which is typical for oceanographic flows. In this case, one may expand the eigenvalues in terms of $1 - r$ and $u_2 - u_1$ to obtain their first-order approximations:

$$\begin{aligned} &\lambda_{1,2}(h_1, u_1, h_2, u_2) \approx U_m \pm \sqrt{g(h_1 + h_2)},\\ &\lambda_{3,4}(h_1, u_1, h_2, u_2) \approx U_c \pm \sqrt{(1-r)g\frac{h_1 h_2}{h_1 + h_2}\left(1 - \frac{(u_2 - u_1)^2}{(1-r)g(h_1 + h_2)}\right)}, \end{aligned} \tag{2.20}$$

where

$$U_m = \frac{h_1 u_1 + h_2 u_2}{h_1 + h_2}, \qquad U_c = \frac{h_1 u_2 + h_2 u_1}{h_1 + h_2}.$$

Similar approximations were obtained in [32].

Remark 2.1. It is clear from (2.20) that the system (2.1) will be hyperbolic provided

$$(u_2 - u_1)^2 < (1 - r)g(h_1 + h_2), \tag{2.21}$$

which means that (2.1) is only conditionally hyperbolic.

Notice that if the condition (2.21) is not satisfied, one cannot compute the local speeds using (2.18). However, the system (2.1) may be still hyperbolic since (2.20) is valid only when $u_1 \sim u_2$ and $r \sim 1$, or it may be in a "weakly" elliptic regime in the sense that it may be stabilized by adding some numerical viscosity. The latter can be achieved, for example, by overestimating the local speeds $a^{\pm}_{j+\frac{1}{2}}$: one may replace the first-order approximations of the largest and smallest eigenvalues of $\frac{\partial \mathbf{F}}{\partial \mathbf{U}}$ by an upper and lower bound, respectively. To this end, we rewrite the characteristic equation (2.19) in the form

$$\lambda^4 + c_1\lambda^3 + c_2\lambda^2 + c_3\lambda + c_4 = 0, \tag{2.22}$$

with coefficients

$$\begin{aligned} &c_1 = -2(u_1+u_2), \quad c_2 = (u_1+u_2)^2 + 2u_1u_2 - g(h_1+h_2),\\ &c_3 = -2u_1u_2(u_1+u_2) + 2g(u_1h_2+u_2h_1),\\ &c_4 = u_1^2u_2^2 - g\left(u_1^2h_2+u_2^2h_1\right) + g^2(1-r)h_1h_2. \end{aligned} \tag{2.23}$$

We then establish the desired bounds on the roots of the polynomial (2.22)–(2.23) using the Lagrange theorem (see, e.g., [29]), according to which the largest nonnegative root is smaller than the sum of the largest and the second largest numbers in the set $\{\sqrt[j]{|c_j|} : j \in J_{\max}\}$, where $\{c_j : j \in J_{\max}\}$ is the set of the negative coefficients of (2.22). Similarly, the smallest nonpositive root of the polynomial (2.22)–(2.23) is larger than the sum of the smallest and the second smallest numbers in the set $\{-\sqrt[j]{|d_j|} : j \in J_{\min}\}$, where $\{d_j : j \in J_{\min}\}$ is the set of negative coefficients of the polynomial

$$\lambda^4 + d_1\lambda^3 + d_2\lambda^2 + d_3\lambda + d_4 = 0, \qquad d_j = (-1)^j c_j \ \forall j.$$

Let us now denote the obtained bounds by $\lambda_{\max} = \lambda_{\max}(h_1, h_2, u_1, u_2)$ and $\lambda_{\min} = \lambda_{\min}(h_1, h_2, u_1, u_2)$. An alternative formula for the one-sided local speeds will then be

$$\begin{aligned} a^+_{j+\frac{1}{2}} &= \max_{\pm}\left\{\lambda_{\max}\left((h_1)^{\pm}_{j+\frac{1}{2}}, (h_2)^{\pm}_{j+\frac{1}{2}}, (u_1)^{\pm}_{j+\frac{1}{2}}, (u_2)^{\pm}_{j+\frac{1}{2}}\right), (u_1)^{\pm}_{j+\frac{1}{2}}, (u_2)^{\pm}_{j+\frac{1}{2}}\right\},\\ a^-_{j+\frac{1}{2}} &= \min_{\pm}\left\{\lambda_{\min}\left((h_1)^{\pm}_{j+\frac{1}{2}}, (h_2)^{\pm}_{j+\frac{1}{2}}, (u_1)^{\pm}_{j+\frac{1}{2}}, (u_2)^{\pm}_{j+\frac{1}{2}}\right), (u_1)^{\pm}_{j+\frac{1}{2}}, (u_2)^{\pm}_{j+\frac{1}{2}}\right\}. \end{aligned} \tag{2.24}$$

2.4. Discretization of the nonconservative products. As we have mentioned in section 1, designing a consistent and stable discretization of nonconservative product terms is a challenging task since a rigorous mathematical theory of systems containing such terms has not been completely developed yet. One may attempt to discretize these terms directly, but this may result in the dependence of the numerical solution of the entire system on the particular discretization. In other words, different nonconservative term discretizations may lead to qualitatively different computed solutions. This is, for example, the case when a central-upwind scheme is applied to the multilayer shallow water system in its original form (1.1). On the other hand, the nonconservative products $g\varepsilon(h_1)_x$ and $-g\varepsilon(\widehat{h}_1)_x$, present in the equivalent system (2.1), are proportional to ε, which is, as indicated in section 1, typically much smaller than the total fluid depth $h_1 + h_2$. Therefore, in the case of oceanographic flows, a numerical solution of (2.1) is expected to be practically nonsensitive to a particular choice of the nonconservative products discretization.

In this paper, we discretize the nonconservative product term $\overline{\mathbf{N}}_j$ (we omit the dependence on t) as follows:

$$\overline{\mathbf{N}}_j^{(2)} = g\cdot\frac{(h_1)^-_{j+\frac12}+w^-_{j+\frac12}+(h_1)^+_{j-\frac12}+w^+_{j-\frac12}}{2}\cdot\frac{(h_1)^-_{j+\frac12}-(h_1)^+_{j-\frac12}}{\Delta x},\quad \overline{\mathbf{N}}_j^{(4)} = -r\cdot\overline{\mathbf{N}}_j^{(2)}. \tag{2.25}$$

2.5. Well-balanced discretization of the geometric source term. A good discretization $\overline{\mathbf{S}}_j$ of the geometric source term should balance the other terms on the RHS of (2.6) so that stationary steady-state solutions $\mathbf{U} = (C_1, 0, C_2, 0)^T$ are preserved, and, thus, the resulting scheme is well-balanced. We follow an argument similar to the one in [19] and [22] to derive a quadrature for $\overline{\mathbf{S}}_j$ that satisfies this property. Note that in the case of stationary steady state (2.20) for the first-order approximation of the eigenvalues reduces to

$$\lambda_{1,2}\approx\pm\sqrt{g(h_1+h_2)},\quad \lambda_{3,4}\approx\pm\sqrt{(1-r)g\frac{h_1h_2}{h_1+h_2}},$$

while the bounds on the largest and smallest eigenvalues obtained by the Lagrange theorem (see page 1750) become

$$\lambda_{\max}=\sqrt{g(h_1+h_2)},\quad \lambda_{\min}=-\sqrt{g(h_1+h_2)}.$$

Hence, independently of whether the one-sided speeds are calculated using (2.18) or (2.24), they satisfy the relation $a^+_{j+\frac12}=-a^-_{j+\frac12}\ \forall j$. Also, in this case, the end point values of the piecewise linear reconstruction are $\mathbf{U}^{\pm}_{j+\frac12}\equiv((h_1)^{\pm}_{j+\frac12},(q_1)^{\pm}_{j+\frac12},w^{\pm}_{j+\frac12},(q_2)^{\pm}_{j+\frac12})^T=(C_1,0,C_2,0)^T\ \forall j$, and, therefore, the first term on the RHS of (2.6) has the following components (we omit the dependence on t):

$$\begin{aligned}&-\frac{\mathbf{H}^{(i)}_{j+\frac12}-\mathbf{H}^{(i)}_{j-\frac12}}{\Delta x}=0,\quad i=1,2,3,\\ &-\frac{\mathbf{H}^{(4)}_{j+\frac12}-\mathbf{H}^{(4)}_{j-\frac12}}{\Delta x}=g\cdot(C_2+rC_1)\cdot\frac{B_{j+\frac12}-B_{j-\frac12}}{\Delta x},\end{aligned} \tag{2.26}$$

where $B_{j\pm\frac12}$ are defined in (2.3). Notice that for stationary steady states the discretization (2.25) of the nonconservative products will give $\overline{\mathbf{N}}^{(i)}_j=0$, $i=1,2,3,4$, since $(h_1)^-_{j+\frac12}=(h_1)^+_{j-\frac12}$. Hence, to preserve stationary steady states, the nonzero contribution of the fluxes, given in (2.26), must be canceled by the contribution of the geometric source term on the RHS of (2.6), and then the following discretization of the geometric source term (once again, we omit the t-dependence)

$$\overline{\mathbf{S}}^{(4)}_j=-g\cdot\frac{w^-_{j+\frac12}+w^+_{j-\frac12}+\left(\widehat{h}_1\right)^-_{j+\frac12}+\left(\widehat{h}_1\right)^+_{j-\frac12}}{2}\cdot\frac{B_{j+\frac12}-B_{j-\frac12}}{\Delta x} \tag{2.27}$$

will result in a well-balanced central-upwind scheme.

2.6. Properties of the scheme. First, we recall that the proposed discretizations of the geometric source term (section 2.5) and the nonconservative products (section 2.4) guarantee that our scheme is well-balanced. In this section, we will show

that the resulting scheme is also positivity preserving. We assume that the ODE system (2.6) is discretized using the forward Euler method and denote two consecutive time levels by t^n and $t^{n+1} = t + \Delta t$. In general, Δt does not have to be constant in time. If this is the case, Δt should be replaced by $(\Delta t)^n$, but this has no effect on our positivity preserving result.

THEOREM 2.1. *Consider the central-upwind semidiscrete scheme given by* (2.6)–(2.7), (2.25), (2.27) *with* (2.3), (2.9)–(2.16), *and either* (2.18) *or* (2.24) *for the two-layer shallow water system* (2.1). *Assume that the system of ODEs* (2.6) *is numerically integrated by the forward Euler method and that for all* j, $(\overline{h_1})_j^n \geq 0$ *and* $(\overline{h_2})_j^n := \overline{w}_j^n - B_j \geq 0$, *where* B_j *are given by* (2.4).

Then, the depth of each layer remains nonnegative in time; that is, $(\overline{h_1})_j^{n+1} \geq 0$ *and* $(\overline{h_2})_j^{n+1} := \overline{w}_j^{n+1} - B_j \geq 0$, *for all* j, *provided that* $\Delta t \leq \Delta x/(2a)$, *where* $a := \max_j\{\max\{a^+_{j+\frac12}, -a^-_{j+\frac12}\}\}$.

Proof. Applying the forward Euler method to the first and the third components of the ODE system (2.6) results in the following:

$$\left(\overline{h_1}\right)_j^{n+1} = \left(\overline{h_1}\right)_j^{n} - \lambda\left(\mathbf{H}^{(1)}_{j+\frac12} - \mathbf{H}^{(1)}_{j-\frac12}\right), \tag{2.28}$$

$$\overline{w}_j^{n+1} = \overline{w}_j^{n} - \lambda\left(\mathbf{H}^{(3)}_{j+\frac12} - \mathbf{H}^{(3)}_{j-\frac12}\right), \tag{2.29}$$

where $\lambda := \Delta t/\Delta x$ and the numerical fluxes are evaluated at time $t = t^n$.

We first show that if the cell averages $(\overline{h_1})_j^n$ are nonnegative, then the new cell averages $(\overline{h_1})_j^{n+1}$ are also nonnegative. Since, according to (2.7) and (2.5), the first component $\mathbf{H}^{(1)}_{j+\frac12}$ of the central-upwind numerical flux is given by

$$\mathbf{H}^{(1)}_{j+\frac12} = \frac{a^+_{j+\frac12}(q_1)^-_{j+\frac12} - a^-_{j+\frac12}(q_1)^+_{j+\frac12}}{a^+_{j+\frac12} - a^-_{j+\frac12}} + \frac{a^+_{j+\frac12}a^-_{j+\frac12}}{a^+_{j+\frac12} - a^-_{j+\frac12}}\Big[(h_1)^+_{j+\frac12} - (h_1)^-_{j+\frac12}\Big], \tag{2.30}$$

we use (2.16) and (2.30) to rewrite (2.28) as

$$\begin{aligned}
(\overline{h_1})_j^{n+1} = {} & \left[\frac12 + \lambda a^-_{j-\frac12}\left(\frac{a^+_{j-\frac12} - (u_1)^+_{j-\frac12}}{a^+_{j-\frac12} - a^-_{j-\frac12}}\right)\right](h_1)^+_{j-\frac12} \\
& + \left[\frac12 - \lambda a^+_{j+\frac12}\left(\frac{(u_1)^-_{j+\frac12} - a^-_{j+\frac12}}{a^+_{j+\frac12} - a^-_{j+\frac12}}\right)\right](h_1)^-_{j+\frac12} \\
& - \lambda a^-_{j+\frac12}\left(\frac{a^+_{j+\frac12} - (u_1)^+_{j+\frac12}}{a^+_{j+\frac12} - a^-_{j+\frac12}}\right)(h_1)^+_{j+\frac12} \\
& + \lambda a^+_{j-\frac12}\left(\frac{(u_1)^-_{j-\frac12} - a^-_{j-\frac12}}{a^+_{j-\frac12} - a^-_{j-\frac12}}\right)(h_1)^-_{j-\frac12},
\end{aligned} \tag{2.31}$$

where we have used the fact that $(\overline{h_1})_j^n = ((h_1)^+_{j-\frac12} + (h_1)^-_{j+\frac12})/2$. Now, the use of a positivity preserving (for example, the generalized minmod (2.8)–(2.11)) piecewise linear reconstruction $\widetilde{h_1}$ ensures that all $(h_1)^\pm_{j\pm\frac12} \geq 0$. On the other hand, it follows from the formulas for the one-sided local speeds (2.18) or (2.24) that $a^+_{j\pm\frac12} \geq 0$,

$a^-_{j\pm\frac12}\le 0$, and

$$0\le\frac{(u_1)^-_{j\pm\frac12}-a^-_{j\pm\frac12}}{a^+_{j\pm\frac12}-a^-_{j\pm\frac12}}\le 1,\quad 0\le\frac{a^+_{j\pm\frac12}-(u_1)^+_{j\pm\frac12}}{a^+_{j\pm\frac12}-a^-_{j\pm\frac12}}\le 1.$$

Therefore, the last two terms in (2.31) are nonnegative. The first two terms in (2.31) will be also nonnegative under the CFL restriction $\lambda a\le 1/2$, where $a:=\max_j\{\max\{a^+_{j+\frac12},-a^-_{j+\frac12}\}\}$. Hence, $(\overline{h_1})^{n+1}_j\ge 0\ \forall j$, since these values are linear combinations of nonnegative point values of $\widetilde{h}_1$ with nonnegative coefficients; see (2.31).

Next, we show that the cell averages $(\overline{h_2})^{n+1}_j$ remain nonnegative if they were nonnegative at the previous time step. The flux component $\mathbf{H}^{(3)}_{j+\frac12}$, given by (see (2.7) and (2.5))

$$\mathbf{H}^{(3)}_{j+\frac12}=\frac{a^+_{j+\frac12}(q_2)^-_{j+\frac12}-a^-_{j+\frac12}(q_2)^+_{j+\frac12}}{a^+_{j+\frac12}-a^-_{j+\frac12}}+\frac{a^+_{j+\frac12}a^-_{j+\frac12}}{a^+_{j+\frac12}-a^-_{j+\frac12}}\left[w^+_{j+\frac12}-w^-_{j+\frac12}\right]$$

can be rewritten using (2.12) as

$$\mathbf{H}^{(3)}_{j+\frac12}=\frac{a^+_{j+\frac12}(q_2)^-_{j+\frac12}-a^-_{j+\frac12}(q_2)^+_{j+\frac12}}{a^+_{j+\frac12}-a^-_{j+\frac12}}+\frac{a^+_{j+\frac12}a^-_{j+\frac12}}{a^+_{j+\frac12}-a^-_{j+\frac12}}\left[(h_2)^+_{j+\frac12}-(h_2)^-_{j+\frac12}\right].\tag{2.32}$$

Notice that since

$$\overline{w}^n_j=\frac12\left(w^+_{j-\frac12}+w^-_{j+\frac12}\right)\quad\text{and}\quad\overline{B}_j=B_j=\frac12\left(B_{j+\frac12}+B_{j-\frac12}\right),$$

we have

$$\left(\overline{h_2}\right)^n_j=\overline{w}^n_j-B_j=\frac{w^+_{j-\frac12}+w^-_{j+\frac12}}{2}-\frac{B_{j-\frac12}+B_{j+\frac12}}{2}=\frac12(h_2)^+_{j-\frac12}+\frac12(h_2)^-_{j+\frac12}.\tag{2.33}$$

Now, we subtract B_j from both sides of (2.29) and use (2.32), (2.16), and (2.33) to derive a formula similar to (2.31):

$$\begin{aligned}(\overline{h_2})^{n+1}_j=&\left[\frac12+\lambda a^-_{j-\frac12}\left(\frac{a^+_{j-\frac12}-(u_2)^+_{j-\frac12}}{a^+_{j-\frac12}-a^-_{j-\frac12}}\right)\right](h_2)^+_{j-\frac12}\\&+\left[\frac12-\lambda a^+_{j+\frac12}\left(\frac{(u_2)^-_{j+\frac12}-a^-_{j+\frac12}}{a^+_{j+\frac12}-a^-_{j+\frac12}}\right)\right](h_2)^-_{j+\frac12}\\&-\lambda a^-_{j+\frac12}\left(\frac{a^+_{j+\frac12}-(u_2)^+_{j+\frac12}}{a^+_{j+\frac12}-a^-_{j+\frac12}}\right)(h_2)^+_{j+\frac12}+\lambda a^+_{j-\frac12}\left(\frac{(u_2)^-_{j-\frac12}-a^-_{j-\frac12}}{a^+_{j-\frac12}-a^-_{j-\frac12}}\right)(h_2)^-_{j-\frac12}.\end{aligned}\tag{2.34}$$

Next, we argue as in the case of $(\overline{h_1})^{n+1}_j$, since

$$0\le\frac{(u_2)^-_{j\pm\frac12}-a^-_{j\pm\frac12}}{a^+_{j\pm\frac12}-a^-_{j\pm\frac12}}\le 1,\quad 0\le\frac{a^+_{j\pm\frac12}-(u_2)^+_{j\pm\frac12}}{a^+_{j\pm\frac12}-a^-_{j\pm\frac12}}\le 1$$

and since the corrected reconstruction for $\widetilde{w}$ guarantees that $(h_2)^\pm_{j\pm\frac12}\ge 0$ (see section 2.3). Thus, the proof is completed. □

Remark 2.2. Theorem 2.1 is still valid if one uses a higher-order SSP ODE solver (either the Runge–Kutta or the multistep one), because such solvers can be written as a convex combination of several forward Euler steps (see [16, 33, 34] for details).

TABLE 2.1
L^1-errors and numerical orders of accuracy.

Number of	ε		h_1	
grid cells	L^1-error	Order	L^1-error	Order
100	9.21e-06	–	7.56e-04	–
200	3.34e-06	1.46	2.18e-04	1.80
400	1.04e-06	1.69	6.01e-05	1.86
800	1.39e-07	2.90	1.46e-05	2.04
1600	3.70e-08	1.91	3.89e-06	1.91

2.7. Numerical experiments. In this section, we test our 1-D scheme on a number of numerical examples. The solutions of the problems solved in sections 2.7.1, 2.7.2, and 2.7.3 are in the hyperbolic regime, and, therefore, the local speeds are calculated using (2.18); the parameter θ, used in the calculation of the numerical derivatives in (2.10), is $\theta = 1$. In sections 2.7.4 and 2.7.5, the velocities difference $u_1 - u_2$ may become relatively large so that the first-order eigenvalues approximation (2.20) will not be valid. Therefore, we overestimate the local speeds using (2.24). In the latter examples, we take $\theta = 2$ in order to reduce the amount of extra numerical diffusion added to the scheme as a result of overestimating the local speeds.

2.7.1. Experimental order of accuracy. The goal of the first numerical example is to experimentally verify the order of accuracy of the proposed central-upwind scheme. The scheme is applied to the system (2.1) with gravitational constant $g = 9.812$ subject to the following initial data and bottom topography:

$$h_1(x,0) = 5 + e^{\cos(2\pi x)}, \quad w(x,0) = -5 - e^{\cos(2\pi x)}, \quad q_1(x,0) \equiv q_2(x,0) \equiv 0,$$
$$B(x) = \sin^2(\pi x) - 10,$$

and 1-periodic boundary conditions. This initial-boundary value problem is a modification of the accuracy test problem, proposed in [37] for the single-layer shallow water equations.

We compute the solution up to time $t = 0.1$ and use the solution computed with 16000 cells over a period as a reference solution. The L^1-errors (over one period) for $\varepsilon = h_1 + h_2 + B$ and h_1 are shown in Table 2.1, where one can clearly observe the experimental second order of accuracy.

2.7.2. Small perturbation of a stationary steady-state solution. We now demonstrate the ability of the developed central-upwind scheme to capture quasi steady states. This example is a two-layer modification of Example 1 from [19].

The initial data, corresponding to a small perturbation of a stationary steady state, are

$$(h_1(x,0), q_1(x,0), w(x,0), q_2(x,0)) = \begin{cases} (1.00001, 0, -1, 0) & \text{if } \ 0.1 < x < 0.2, \\ (1.00000, 0, -1, 0) & \text{otherwise,} \end{cases}$$

the gravitational constant is $g = 10$, the density ratio is $r = 0.98$, and the bottom topography is

$$B(x) = \begin{cases} 0.25\,[\cos(10\pi(x - 0.5)) + 1] - 2 & \text{if } \ 0.4 < x < 0.6, \\ -2 & \text{otherwise.} \end{cases} \tag{2.35}$$

We compute the numerical solution on a sequence of uniform grids with $\Delta x = 1/100$, $1/200$, and $1/1600$ (the latter one serves as a reference solution for this numerical experiment since the exact solution is unavailable). In Figure 2.1 (left), we present

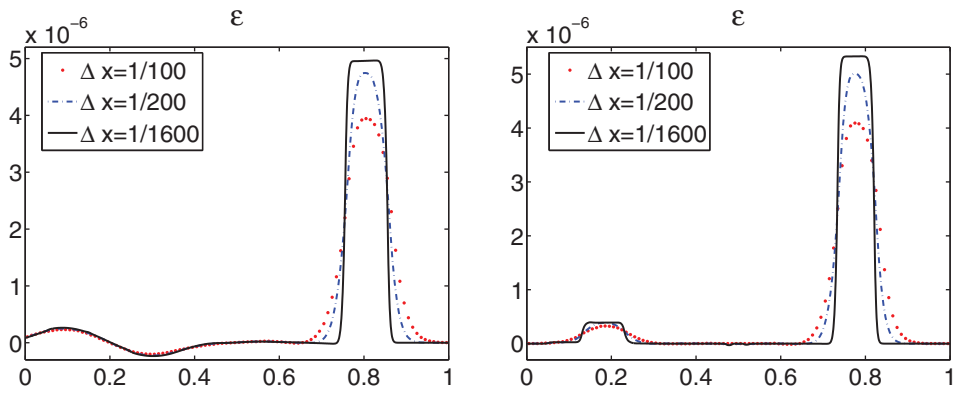

FIG. 2.1. *Propagation of a small perturbation of a stationary steady state over the smooth bottom given by* (2.35), *left, and the discontinuous bottom given by* (2.36), *right: water surface* ε.

the fluctuation of the water level $\varepsilon = h_1 + h_2 + B$ at time $t = 0.15$. As expected, no oscillations were produced by our well-balanced scheme.

We also consider the same example but with the discontinuous bottom topography:

$$B(x) = \begin{cases} -1.5 & \text{if } \ x > 0.5, \\ -2.0 & \text{otherwise.} \end{cases} \tag{2.36}$$

Once again, we compute the numerical solution at time $t = 0.15$ on a sequence of uniform grids with $\Delta x = 1/100$, $1/200$, and $1/1600$ and present the water surface in Figure 2.1 (right).

Even though the bottom topography function is discontinuous now, the obtained solution is still oscillation-free thanks to the well-balanced property of the scheme.

2.7.3. Interface propagation. In this section, we numerically study the propagation of the interface. We consider two examples.

The first example is taken from [1] and is a slight modification of test problem 2 from [5]. The goal here is to capture the propagation of the interface, initially located at $x = 0.3$:

$$(h_1(x,0), q_1(x,0), h_2(x,0), q_2(x,0)) = \begin{cases} (0.50, 1.250, 0.50, 1.250) & \text{if } \ x < 0.3, \\ (0.45, 1.125, 0.55, 1.375) & \text{if } \ x > 0.3. \end{cases}$$

The bottom in this example is flat ($B \equiv -1$), the gravitational constant is $g = 10$, and the density ratio is $r = 0.98$.

We compute the numerical solution at time $t = 0.1$ on a sequence of uniform grids with $\Delta x = 1/100$, $1/200$, $1/400$, $1/800$, and $1/10000$ (the latter one serves as a reference solution for this numerical experiment since the exact solution is unavailable). The obtained results are shown in Figures 2.2–2.4. As one may clearly see in Figure 2.2 (left), the low resolution calculations suggest that the interface remains sharp while propagating to the right and being diffused due to the numerical viscosity (similar low resolution results were reported in [5]). However, when the grid is refined (see Figure 2.2 (right)) and the influence of numerical diffusion is reduced, the shape of the interface looks completely different: we can now see that an intermediate flat state ($h_1 \approx 0.475$) has emerged. It is connected to the left ($h_1 = 0.5$) and right ($h_1 = 0.45$) states through two waves that seem to be shock discontinuities.

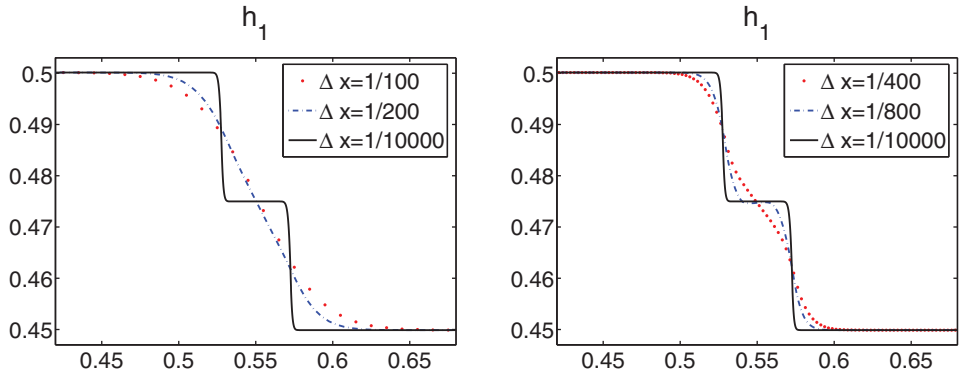

FIG. 2.2. *Interface propagation problem, first example: h_1-component of the solution, zoom at the interface area.*

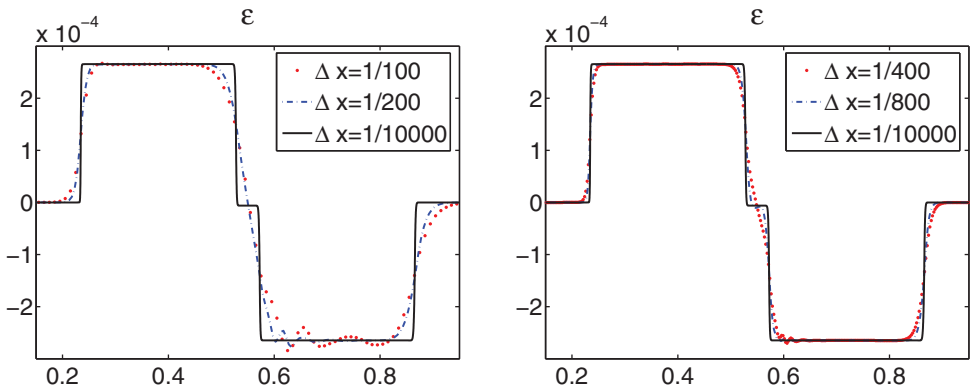

FIG. 2.3. *Interface propagation problem, first example: water surface ε.*

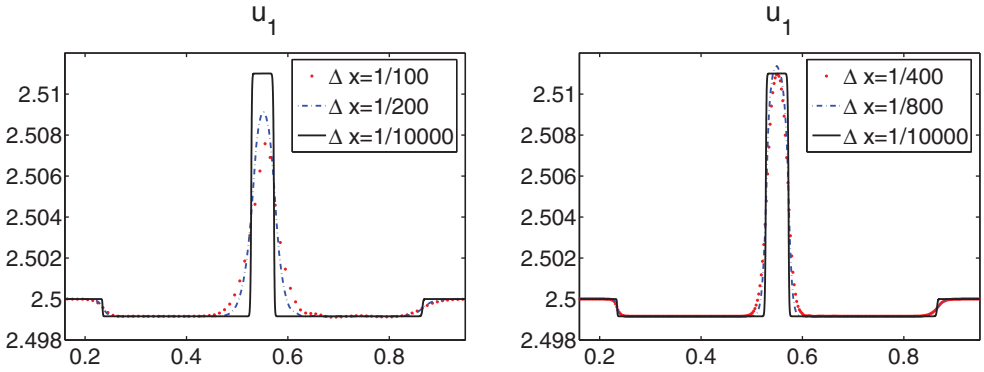

FIG. 2.4. *Interface propagation problem, first example: velocity of the upper layer u_1.*

As expected, the initial sharp interface produces 4 waves traveling with 4 different characteristic speeds. This can be clearly seen in Figures 2.3–2.4, where we plot the water surface ε and the velocity of the upper layer u_1. Notice that the low resolution calculation of ε (Figure 2.3 (left)) produces some "ENO-type" oscillations which disappear when the grid is refined (Figure 2.3 (right)).

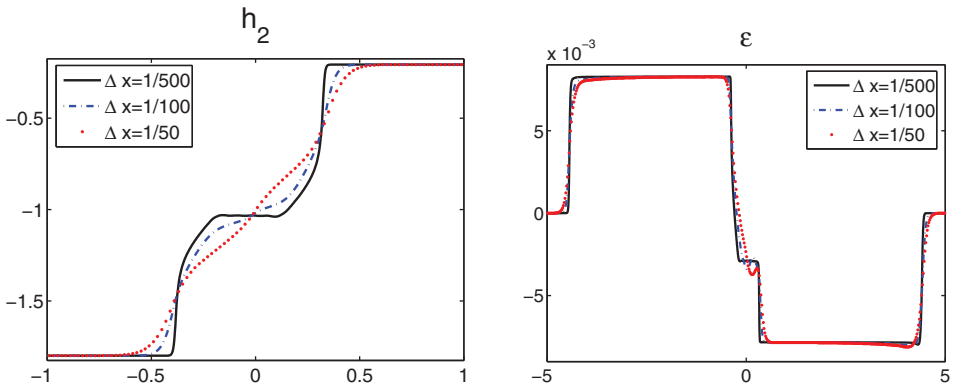

FIG. 2.5. *Interface propagation problem, second example: h_2-component of the solution zoomed at the interface area (left) and water surface ε (right).*

Next, we consider a more complicated example with a much larger initial jump at the interface:

$$(h_1(x,0),q_1(x,0),h_2(x,0),q_2(x,0)) = \begin{cases} (1.8,0,0.2,0) & \text{if } x<0,\\ (0.2,0,1.8,0) & \text{if } x>0. \end{cases}$$

The bottom topography is flat ($B \equiv -2$), the gravitational constant is $g = 9.81$, and the density ratio is $r = 0.98$.

This example is taken from [4] (see also [31]). The time-splitting scheme proposed there produces a stationary shock (see Figure 7 in [4]), which seems to be unphysical. The solutions computed by our central-upwind scheme on three different grids with $\Delta x = 1/50, 1/100$, and $1/500$ do not contain such a shock. This can be clearly seen in Figure 2.5, where h_2 and ε, computed at time $t = 1$, are shown.

2.7.4. Lock exchange problem. In this example, taken from [6], the two layers are initially separated—the lighter water is on the left, while the heavier one is on the right:

$$(h_1(x,0),q_1(x,0),h_2(x,0),q_2(x,0)) = \begin{cases} (-B(x),0,0,0) & \text{if } x<0,\\ (0,0,-B(x),0) & \text{if } x>0, \end{cases}$$

where the bottom topography is the Gaussian-shape function

$$B(x) = e^{-x^2} - 2$$

(the initial setting is shown in Figure 2.6 (left)). The gravitational constant is $g = 9.81$, and the density ratio is $r = 0.98$. The computational domain is $[-3, 3]$, and the boundary conditions are $q_1 = -q_2$ at each end of the interval.

In this initial-boundary value problem, the heavier water propagates to the left, while the lighter one moves to the right. The solution is expected to converge to a smooth nonstationary steady state. The analytical steady-state solution is unavailable. However, one may obtain a rigid lid approximation of it; see, e.g., [12, 14].

We compute a numerical steady-state solution on a uniform grid with $\Delta x = 0.02$. The obtained results, shown in Figure 2.6 (right), are very similar to the ones obtained in [6]. We note that no interface instabilities have been observed in this example, even though initially $h_1 = 0$ for $x > 0$ and $h_2 = 0$ for $x < 0$, and, at small times, either h_1 or h_2 is (almost) zero in a significant part of the computational domain. One of the

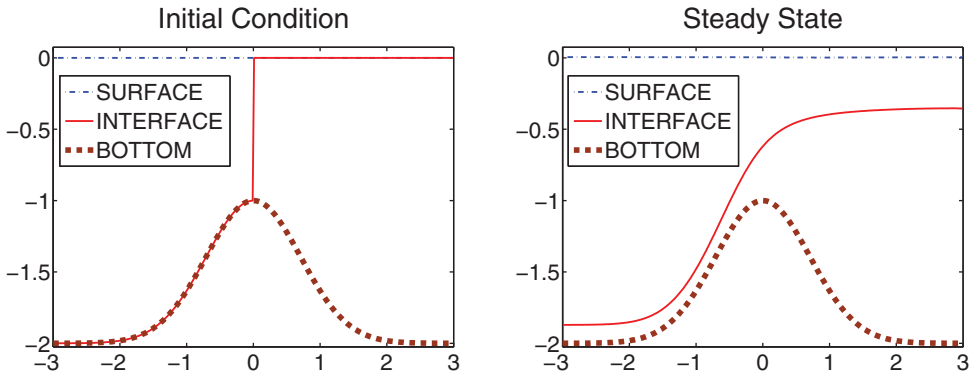

FIG. 2.6. *Lock exchange problem: water surface ε, interface w, and bottom topography B.*

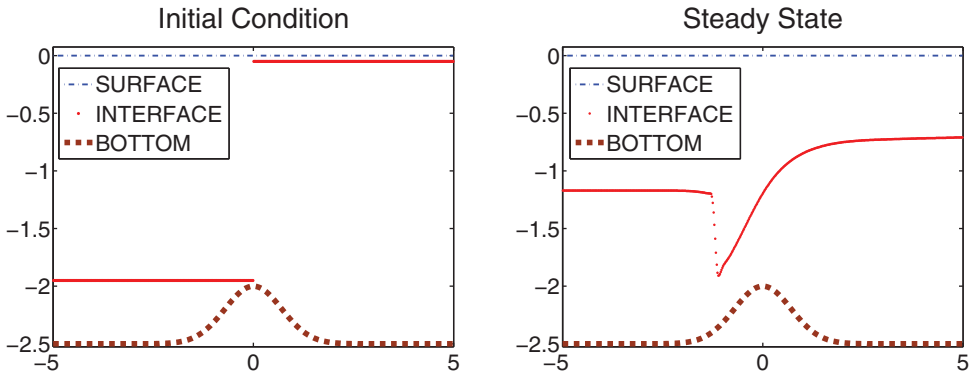

FIG. 2.7. *Internal dam break problem: water surface ε, interface w, and bottom topography B.*

key stability factors here is the ability of our scheme to preserve the positivity of each layer depth, as proved in Theorem 2.1.

2.7.5. Internal dam break. In this example, we model an internal dam break over a nonflat bottom by considering the following initial data:

$$(h_1(x,0), q_1(x,0), h_2(x,0), q_2(x,0)) = \begin{cases} (1.95, 0, -1.95 - B(x), 0) & \text{if } x < 0, \\ (0.05, 0, -0.05 - B(x), 0) & \text{if } x > 0 \end{cases}$$

and bottom topography function

$$B(x) = 0.5e^{-x^2} - 2.5$$

(see Figure 2.7 (left)). The gravitational constant is $g = 9.81$, and the density ratio is $r = 0.998$. We take a sufficiently large computational domain $[-5, 5]$ and impose free boundary conditions at each end of it.

As in the previous example, the solution of the studied initial-boundary value problem is expected to converge to a steady state. Unlike the previous example, the steady-state solution will now contain a hydraulic jump, which makes this test problem even more challenging.

We compute a numerical steady-state solution on a uniform grid with $\Delta x = 0.02$. The obtained results are shown in Figure 2.7 (right). One can observe a high overall

resolution of the discontinuous interface, achieved by the proposed central-upwind scheme.

3. Two-dimensional scheme. Similar to the 1-D case, we first introduce the new variable $w := h_2 + B$ and rewrite the 2-D system (1.2) in terms of the unknowns $\mathbf{U} := (h_1, q_1, p_1, w, q_2, p_2)$ in the following way:

$$
\begin{cases}
(h_1)_t + (q_1)_x + (p_1)_y = 0,\\
(q_1)_t + \left[\dfrac{q_1^2}{h_1} + gh_1\varepsilon\right]_x + \left(\dfrac{q_1p_1}{h_1}\right)_y = g\varepsilon(h_1)_x,\\
(p_1)_t + \left(\dfrac{q_1p_1}{h_1}\right)_x + \left[\dfrac{p_1^2}{h_1} + gh_1\varepsilon\right]_y = g\varepsilon(h_1)_y,\\
w_t + (q_2)_x + (p_2)_y = 0,\\
(q_2)_t + \left[\dfrac{q_2^2}{w-B} + \dfrac{g}{2}w^2 - \dfrac{g}{2}rh_1^2 - gB\widehat{\varepsilon}\right]_x + \left(\dfrac{q_2p_2}{w-B}\right)_y = -g\varepsilon\left(\widehat{h}_1\right)_x - g\widehat{\varepsilon}B_x,\\
(p_2)_t + \left(\dfrac{q_2p_2}{w-B}\right)_x + \left[\dfrac{p_2^2}{w-B} + \dfrac{g}{2}w^2 - \dfrac{g}{2}rh_1^2 - gB\widehat{\varepsilon}\right]_y = -g\varepsilon\left(\widehat{h}_1\right)_y - g\widehat{\varepsilon}B_y,
\end{cases}
\tag{3.1}
$$

where $\varepsilon := h_1 + w = h_1 + h_2 + B$ and $\widehat{\varepsilon} := \widehat{h}_1 + w$. While it can be easily shown that the systems (3.1) and (1.2) are equivalent for smooth solutions, as in the 1-D case, there is no complete mathematical theory of weak solutions for either of them. We claim that the system (3.1) is more suitable for numerical computations for at least two reasons. First, similar to the 1-D case, this formulation helps to design well-balanced numerical schemes, namely, the schemes that exactly preserve stationary steady-states solutions satisfying

$$q_1 = p_1 = q_2 = p_2 \equiv 0, \quad h_1 \equiv \text{const}, \quad w \equiv \text{const}.$$

Second, the presence of the small factor ε in the nonconservative products $g\varepsilon(h_1)_x$, $g\varepsilon(h_1)_y$, $-g\varepsilon(\widehat{h}_1)_x$, and $-g\varepsilon(\widehat{h}_1)_y$ reduces their influence and makes the computed solution practically independent of the choice of their discretization.

We solve the system (3.1) using a modification of the well-balanced positivity preserving scheme, developed in [22] in the context of the single-layer shallow water equations. Similar to the 1-D case, we use a uniform grid with $x_\alpha = \alpha\Delta x$ and $y_\beta = \beta\Delta y$, where Δx and Δy are small spatial scales, and denote by $C_{j,k}$ the computational cell $C_{j,k} := [x_{j-\frac12}, x_{j+\frac12}] \times [y_{k-\frac12}, y_{k+\frac12}]$.

3.1. Bottom discretization. We start the description of our well-balanced positivity preserving central-upwind scheme for the system (3.1) by replacing the bottom topography function B with its continuous piecewise bilinear approximation $\widetilde{B}$, which at each cell $C_{j,k}$ is given by the following bilinear form:

$$
\begin{aligned}
\widetilde{B}(x,y) = B_{j-\frac12,k-\frac12} &+ \left(B_{j+\frac12,k-\frac12} - B_{j-\frac12,k-\frac12}\right)\cdot\frac{x - x_{j-\frac12}}{\Delta x}\\
&+ \left(B_{j-\frac12,k+\frac12} - B_{j-\frac12,k-\frac12}\right)\cdot\frac{y - y_{k-\frac12}}{\Delta y}\\
&+ \left(B_{j+\frac12,k+\frac12} - B_{j+\frac12,k-\frac12} - B_{j-\frac12,k+\frac12} + B_{j-\frac12,k-\frac12}\right)\\
&\quad\cdot\frac{\left(x - x_{j-\frac12}\right)\left(y - y_{k-\frac12}\right)}{\Delta x\Delta y}, \quad (x,y) \in C_{j,k}.
\end{aligned}
\tag{3.2}
$$

Here, $B_{j\pm\frac12,k\pm\frac12}$ are the values of $\widetilde{B}$ at the corners of the cell $C_{j,k}$, defined as

$$B_{j\pm\frac12,k\pm\frac12}:=\frac12\Bigg(\max_{\xi^2+\eta^2=1}\lim_{h,\ell\to0}B\left(x_{j\pm\frac12}+h\xi,y_{k\pm\frac12}+\ell\eta\right)+\min_{\xi^2+\eta^2=1}\lim_{h,\ell\to0}B\left(x_{j\pm\frac12}+h\xi,y_{k\pm\frac12}+\ell\eta\right)\Bigg).$$

This formula reduces to $B_{j\pm\frac12,k\pm\frac12}=B(x_{j\pm\frac12},y_{k\pm\frac12})$ if the function B is continuous at $(x_{j\pm\frac12},y_{k\pm\frac12})$. As in the 1-D case, we note that replacing B with $\widetilde{B}$ does not affect the (formal) order of the central-upwind scheme since the piecewise bilinear interpolant (3.2) is (formally) a second-order approximant to B.

Note that the restriction of the interpolant $\widetilde{B}$ along each of the lines $x=x_j$ or $y=y_k$ is a continuous piecewise linear function, and, as in the 1-D case (see (2.4)), the cell average of $\widetilde{B}$ over the cell $C_{j,k}$ is equal to its value at the center of the cell and is also equal to the average of the values of $\widetilde{B}$ at the midpoints of the edges of $C_{j,k}$, namely, we have

$$\begin{aligned}B_{j,k}:=\widetilde{B}(x_j,y_k)&=\frac{1}{\Delta x\Delta y}\iint_{C_{j,k}}\widetilde{B}(x,y)\,dx\,dy\\&=\frac14\left(B_{j+\frac12,k}+B_{j-\frac12,k}+B_{j,k+\frac12}+B_{j,k-\frac12}\right)\\&=\frac12\left(B_{j+\frac12,k}+B_{j-\frac12,k}\right)=\frac12\left(B_{j,k+\frac12}+B_{j,k-\frac12}\right),\end{aligned}\tag{3.3}$$

where

$$\begin{aligned}B_{j+\frac12,k}&:=\widetilde{B}(x_{j+\frac12},y_k)=\frac12\left(B_{j+\frac12,k+\frac12}+B_{j+\frac12,k-\frac12}\right),\\B_{j,k+\frac12}&:=\widetilde{B}(x_j,y_{k+\frac12})=\frac12\left(B_{j+\frac12,k+\frac12}+B_{j-\frac12,k+\frac12}\right).\end{aligned}\tag{3.4}$$

Formulae (3.3)–(3.4) are crucial for the proof of the positivity preserving property of our 2-D well-balanced central-upwind scheme (see Theorem 3.1). Notice that, in general, $B_{j+\frac12,k}\neq B(x_{j+\frac12},y_k)$ and $B_{j,k+\frac12}\neq B(x_j,y_{k+\frac12})$ even when B is continuous.

3.2. Semidiscrete central-upwind scheme. Before describing the scheme, we introduce the vector notations $\mathbf{F}$ and $\mathbf{G}$ for the fluxes

$$\mathbf{F}(\mathbf{U},B):=\left(q_1,\frac{q_1^2}{h_1}+gh_1\varepsilon,\frac{q_1p_1}{h_1},q_2,\frac{q_2^2}{w-B}+\frac12gw^2-\frac12gr\widehat{h}_1^2-gB\widehat{\varepsilon},\frac{q_2p_2}{w-B}\right)^T,$$

$$\mathbf{G}(\mathbf{U},B):=\left(p_1,\frac{q_1p_1}{h_1},\frac{p_1^2}{h_1}+gh_1\varepsilon,p_2,\frac{q_2p_2}{w-B},\frac{p_2^2}{w-B}+\frac12gw^2-\frac12gr\widehat{h}_1^2-gB\widehat{\varepsilon}\right)^T,$$

$\mathbf{N}$ for the nonconservative products

$$\mathbf{N}(\mathbf{U},B):=\left(0,g\varepsilon(h_1)_x,g\varepsilon(h_1)_y,0,-g\varepsilon\left(\widehat{h}_1\right)_x,-g\varepsilon\left(\widehat{h}_1\right)_y\right)^T,$$

and $\mathbf{S}$ for the source term $\mathbf{S}(\mathbf{U},B) := (0,0,0,0,-gB_x\widehat{\varepsilon},-gB_y\widehat{\varepsilon})^T$. Using these notations, a central-upwind semidiscretization of (3.1) can be written as the following system of time-dependent ODEs (see [21, 22, 24] for details):

$$\begin{aligned}\frac{d}{dt}\overline{\mathbf{U}}_{j,k}(t) = &-\frac{\mathbf{H}^x_{j+\frac12,k}(t)-\mathbf{H}^x_{j-\frac12,k}(t)}{\Delta x}-\frac{\mathbf{H}^y_{j,k+\frac12}(t)-\mathbf{H}^y_{j,k-\frac12}(t)}{\Delta y}\\ &+\overline{\mathbf{S}}_{j,k}(t)+\overline{\mathbf{N}}_{j,k}(t),\end{aligned}\tag{3.5}$$

where the evolved quantities $\overline{\mathbf{U}}_{j,k}$ are approximations of the cell averages over the corresponding cells:

$$\overline{\mathbf{U}}_{j,k}(t)\approx\frac{1}{\Delta x\Delta y}\iint_{C_{j,k}}\mathbf{U}(x,y,t)\,dx\,dy.$$

In (3.5), $\overline{\mathbf{S}}_{j,k}$ and $\overline{\mathbf{N}}_{j,k}$ stand for the discretizations of the source and nonconservative product terms, respectively,

$$\begin{aligned}\overline{\mathbf{S}}_{j,k}(t)&\approx\frac{1}{\Delta x\Delta y}\iint_{C_{j,k}}\mathbf{S}(\mathbf{U}(x,y,t),B(x,y))\,dx\,dy,\\ \overline{\mathbf{N}}_{j,k}(t)&\approx\frac{1}{\Delta x\Delta y}\iint_{C_{j,k}}\mathbf{N}(\mathbf{U}(x,y,t),B(x,y))\,dx\,dy\end{aligned}$$

(the details are provided in sections 3.4 and 3.5), and the numerical fluxes $\mathbf{H}^x$ and $\mathbf{H}^y$ are given by (see [21, 22, 24] for their rigorous derivation)

$$\begin{aligned}\mathbf{H}^x_{j+\frac12,k}=&\frac{a^+_{j+\frac12,k}\mathbf{F}\left(\mathbf{U}^{\mathrm{E}}_{j,k},B_{j+\frac12,k}\right)-a^-_{j+\frac12,k}\mathbf{F}\left(\mathbf{U}^{\mathrm{W}}_{j+1,k},B_{j+\frac12,k}\right)}{a^+_{j+\frac12,k}-a^-_{j+\frac12,k}}\\ &+\frac{a^+_{j+\frac12,k}a^-_{j+\frac12,k}}{a^+_{j+\frac12,k}-a^-_{j+\frac12,k}}\left[\mathbf{U}^{\mathrm{W}}_{j+1,k}-\mathbf{U}^{\mathrm{E}}_{j,k}\right],\\ \mathbf{H}^y_{j,k+\frac12}=&\frac{b^+_{j,k+\frac12}\mathbf{G}\left(\mathbf{U}^{\mathrm{N}}_{j,k},B_{j,k+\frac12}\right)-b^-_{j,k+\frac12}\mathbf{G}\left(\mathbf{U}^{\mathrm{S}}_{j,k+1},B_{j,k+\frac12}\right)}{b^+_{j,k+\frac12}-b^-_{j,k+\frac12}}\\ &+\frac{b^+_{j,k+\frac12}b^-_{j,k+\frac12}}{b^+_{j,k+\frac12}-b^-_{j,k+\frac12}}\left[\mathbf{U}^{\mathrm{S}}_{j,k+1}-\mathbf{U}^{\mathrm{N}}_{j,k}\right],\end{aligned}$$

where $B_{j+\frac12,k}$ and $B_{j,k+\frac12}$ are described in (3.4). Here, $\mathbf{U}^{\mathrm{E,W,N,S}}_{j,k}$ are the point values of the piecewise linear reconstruction $\widetilde{\mathbf{U}}\equiv(\widetilde{h}_1,\widetilde{q}_1,\widetilde{p}_1,\widetilde{w},\widetilde{q}_2,\widetilde{p}_2)^T$ for $\mathbf{U}$,

$$\widetilde{\mathbf{U}}(x,y):=\overline{\mathbf{U}}_{j,k}+(\mathbf{U}_x)_{j,k}(x-x_j)+(\mathbf{U}_y)_{j,k}(y-y_k),\quad(x,y)\in C_{j,k},\tag{3.6}$$

at $(x_{j+\frac12},y_k)$, $(x_{j-\frac12},y_k)$, $(x_j,y_{k+\frac12})$, and $(x_j,y_{k-\frac12})$, respectively. Namely, we have

$$\begin{aligned}
&\mathbf{U}^{\mathrm{E}}_{j,k}:=\widetilde{\mathbf{U}}(x_{j+\frac12}-0,y_k)=\overline{\mathbf{U}}_{j,k}+\tfrac{\Delta x}{2}(\mathbf{U}_x)_{j,k},\\
&\mathbf{U}^{\mathrm{W}}_{j,k}:=\widetilde{\mathbf{U}}(x_{j-\frac12}+0,y_k)=\overline{\mathbf{U}}_{j,k}-\tfrac{\Delta x}{2}(\mathbf{U}_x)_{j,k},\\
&\mathbf{U}^{\mathrm{N}}_{j,k}:=\widetilde{\mathbf{U}}(x_j,y_{k+\frac12}-0)=\overline{\mathbf{U}}_{j,k}+\tfrac{\Delta y}{2}(\mathbf{U}_y)_{j,k},\\
&\mathbf{U}^{\mathrm{S}}_{j,k}:=\widetilde{\mathbf{U}}(x_j,y_{k-\frac12}+0)=\overline{\mathbf{U}}_{j,k}-\tfrac{\Delta y}{2}(\mathbf{U}_y)_{j,k}.
\end{aligned}\tag{3.7}$$

The numerical derivatives $(\mathbf{U}_x)_{j,k}$ and $(\mathbf{U}_y)_{j,k}$ are (at least) first-order componentwise approximations of $\mathbf{U}_x(x_j,y_k,t)$ and $\mathbf{U}_y(x_j,y_k,t)$, respectively. To ensure a nonoscillatory nature of the reconstruction (3.6), the numerical derivatives have to be computed using a nonlinear limiter. The one-sided local speeds in the x- and y-directions $a^{\pm}_{j+\frac12,k}$ and $b^{\pm}_{j,k+\frac12}$ are obtained from the largest and the smallest eigenvalues of the Jacobians $\frac{\partial\mathbf{F}}{\partial\mathbf{U}}$ and $\frac{\partial\mathbf{G}}{\partial\mathbf{U}}$, respectively. As before, we suppress the dependence of $\overline{\mathbf{U}}_{j,k}$, $\mathbf{U}^{\mathrm{E,W,N,S}}_{j,k}$, $(\mathbf{U}_x)_{j,k}$, $(\mathbf{U}_y)_{j,k}$, $a^{\pm}_{j+\frac12,k}$, and $b^{\pm}_{j,k+\frac12}$ on t to simplify the notation.

Finally, the system (3.5) should be solved by a stable ODE solver of an appropriate order. In our numerical experiments, we have used the third-order SSP-RK ODE solver.

3.3. Positivity preserving reconstructions. In this section, we extend the positivity preserving reconstruction, introduced in section 2.3, to two space dimensions. As in the 1-D case, we begin with computing the numerical derivatives $(\mathbf{U}_x)_{j,k}$ and $(\mathbf{U}_y)_{j,k}$ with the help of a nonlinear limiter. In our numerical experiments, we have used the generalized minmod limiter:

$$\begin{aligned}
(\mathbf{U}_x)_{j,k}&=\mathrm{minmod}\left(\theta_1\frac{\overline{\mathbf{U}}_{j,k}-\overline{\mathbf{U}}_{j-1,k}}{\Delta x},\ \frac{\overline{\mathbf{U}}_{j+1,k}-\overline{\mathbf{U}}_{j-1,k}}{2\Delta x},\ \theta_1\frac{\overline{\mathbf{U}}_{j+1,k}-\overline{\mathbf{U}}_{j,k}}{\Delta x}\right),\\
(\mathbf{U}_y)_{j,k}&=\mathrm{minmod}\left(\theta_2\frac{\overline{\mathbf{U}}_{j,k}-\overline{\mathbf{U}}_{j,k-1}}{\Delta y},\ \frac{\overline{\mathbf{U}}_{j,k+1}-\overline{\mathbf{U}}_{j,k-1}}{2\Delta y},\ \theta_2\frac{\overline{\mathbf{U}}_{j,k+1}-\overline{\mathbf{U}}_{j,k}}{\Delta y}\right),
\end{aligned}\tag{3.8}$$

where $\theta_1,\ \theta_2\in[1,2]$. Notice that the generalized minmod reconstruction is positivity preserving in the sense that the use of the numerical derivatives (3.8) in (3.6) guarantees that, as long as $(\overline{h_1})_{j,k}\ge 0\ \forall j,k$, the point values $(h_1)^{\mathrm{E,W,N,S}}_{j,k}\ge 0$. This is true since each of the reconstructed point values is always bounded by the cell averages from the neighboring two cells. However, even a positivity preserving reconstruction for w will not guarantee that $(h_2)^{\mathrm{E,W,N,S}}_{j,k}\ge 0$ since these values are obtained from the corresponding reconstructed values $w^{\mathrm{E,W,N,S}}_{j,k}$ in the following way:

$$\begin{aligned}
&(h_2)^{\mathrm{E}}_{j,k}=w^{\mathrm{E}}_{j,k}-B_{j+\frac12,k},\qquad (h_2)^{\mathrm{W}}_{j,k}=w^{\mathrm{W}}_{j,k}-B_{j-\frac12,k},\\
&(h_2)^{\mathrm{N}}_{j,k}=w^{\mathrm{N}}_{j,k}-B_{j,k+\frac12},\qquad (h_2)^{\mathrm{S}}_{j,k}=w^{\mathrm{S}}_{j,k}-B_{j,k-\frac12}.
\end{aligned}\tag{3.9}$$

As in the 1-D case, a correction of the basic reconstruction (3.6)–(3.8) for w is needed to enforce $(h_2)^{\mathrm{E,W,N,S}}_{j,k}\ge 0$. In fact, we need to correct $\widetilde{w}$ only in the following four

cases:

$$\text{if } \ w^{\mathrm{E}}_{j,k} < B_{j+\frac12,k}, \ \text{ then take } \ (w_x)_{j,k} := \frac{B_{j+\frac12,k} - \overline{w}_{j,k}}{\frac{\Delta x}{2}},$$

$$\Longrightarrow \ w^{\mathrm{E}}_{j,k} = B_{j+\frac12,k}\,, \ \ w^{\mathrm{W}}_{j,k} = 2\overline{w}_{j,k} - B_{j+\frac12,k}; \tag{3.10}$$

$$\text{if } \ w^{\mathrm{W}}_{j,k} < B_{j-\frac12,k}, \ \text{ then take } \ (w_x)_{j,k} := \frac{\overline{w}_{j,k} - B_{j-\frac12,k}}{\frac{\Delta x}{2}},$$

$$\Longrightarrow \ w^{\mathrm{E}}_{j,k} = 2\overline{w}_{j,k} - B_{j-\frac12,k}\,, \ \ w^{\mathrm{W}}_{j,k} = B_{j-\frac12,k}; \tag{3.11}$$

$$\text{if } \ w^{\mathrm{N}}_{j,k} < B_{j,k+\frac12}, \ \text{ then take } \ (w_y)_{j,k} := \frac{B_{j,k+\frac12} - \overline{w}_{j,k}}{\frac{\Delta y}{2}},$$

$$\Longrightarrow \ w^{\mathrm{N}}_{j,k} = B_{j,k+\frac12}\,, \ \ w^{\mathrm{S}}_{j,k} = 2\overline{w}_{j,k} - B_{j,k+\frac12}; \tag{3.12}$$

$$\text{if } \ w^{\mathrm{S}}_{j,k} < B_{j,k-\frac12}, \ \text{ then take } \ (w_y)_{j,k} := \frac{\overline{w}_{j,k} - B_{j,k-\frac12}}{\frac{\Delta y}{2}},$$

$$\Longrightarrow \ w^{\mathrm{N}}_{j,k} = 2\overline{w}_{j,k} - B_{j,k-\frac12}\,, \ \ w^{\mathrm{S}}_{j,k} = B_{j,k-\frac12}. \tag{3.13}$$

The correction procedure (3.10)–(3.13) guarantees that the reconstruction $\widetilde{w}$ is conservative and the graphs of its restrictions on the lines $y = y_k$ and $x = x_j$ are above $\widetilde{B}(x, y_k)$ and $\widetilde{B}(x_j, y)$, respectively. This will assure that the point values of the fluid depth h_2 of the second layer, computed by (3.9), will be nonnegative. As in the 1-D case, the obtained values of h_1 and h_2 may be very small (or even zero). Therefore, the corresponding velocities should be calculated in a way similar to (2.15) (for simplicity, we omit the E, W, S, N, j, and k indexes):

$$u_i = \frac{\sqrt{2}\,q_i h_i}{\sqrt{(h_i)^4 + \max((h_i)^4, \delta)}}, \quad v_i = \frac{\sqrt{2}\,p_i h_i}{\sqrt{(h_i)^4 + \max((h_i)^4, \delta)}}, \quad i = 1, 2, \tag{3.14}$$

where δ is a prescribed tolerance (we have taken $\delta = \max\{(\Delta x)^4, (\Delta y)^4\}$ in all of our computations). After evaluating h_i, u_i, and v_i, we recompute the x- and y-discharges accordingly; that is, we set

$$q_i = h_i \cdot u_i, \quad p_i = h_i \cdot v_i, \quad i = 1, 2, \tag{3.15}$$

at the points where the fluxes are to be calculated.

Next, we compute the local one-sided speeds of propagation. To this end, we need to calculate the eigenvalues of the Jacobians $\frac{\partial \mathbf{F}}{\partial \mathbf{U}}$ and $\frac{\partial \mathbf{G}}{\partial \mathbf{U}}$. Let us consider the first of these Jacobians $\frac{\partial \mathbf{F}}{\partial \mathbf{U}}$. Two of its eigenvalues are equal to u_1 and u_2, and the remaining four eigenvalues are to be determined from the characteristic equation (2.19). The eigenvalues of the second Jacobian $\frac{\partial \mathbf{G}}{\partial \mathbf{U}}$ are equal to v_1 and v_2, and the rest are to be determined from the characteristic equation (2.19) with u_1 and u_2 replaced by v_1 and v_2, respectively. Therefore, we compute the local speeds $a^{\pm}_{j+\frac12,k}$ using either the first-order approximation of the eigenvalues (leading to (2.18) and (2.20)) or their upper and lower bounds (resulting in (2.24)). The only difference is that in the 1-D formulas $(h_i)^+_{j+\frac12}$, $(h_i)^-_{j+\frac12}$, $(u_i)^+_{j+\frac12}$, and $(u_i)^-_{j+\frac12}$ have to be replaced with $(h_i)^{\mathrm{W}}_{j+1,k}$,

$(h_i)^{\rm E}_{j,k}$, $(u_i)^{\rm W}_{j+1,k}$, and $(u_i)^{\rm E}_{j,k}$, respectively $(i=1,2)$. For the computation of $b^{\pm}_{j,k+\frac12}$, we again use either the first-order approximation of the eigenvalues (leading to (2.18) and (2.20)) or their upper and lower bounds (resulting in (2.24)), where $(h_i)^{+}_{j+\frac12}$, $(h_i)^{-}_{j+\frac12}$, $(u_i)^{+}_{j+\frac12}$, and $(u_i)^{-}_{j+\frac12}$ have to be replaced with $(h_i)^{\rm S}_{j,k+1}$, $(h_i)^{\rm N}_{j,k}$, $(v_i)^{\rm S}_{j,k+1}$, and $(v_i)^{\rm N}_{j,k}$, respectively $(i=1,2)$.

3.4. Discretization of the nonconservative products. As pointed out in the beginning of section 3, the purpose of rewriting the two-layer shallow water system in the form (3.1) is to minimize the effect of the discretization of the nonconservative product terms on the behavior of the computed solution. Here, we use the 2-D extension of the 1-D discretization from section 2.4 (the dependence on t is omitted):

$$\begin{aligned}
&\overline{\mathbf{N}}^{(2)}_{j,k}=g\frac{(h_1)^{\rm E}_{j,k}+w^{\rm E}_{j,k}+(h_1)^{\rm W}_{j,k}+w^{\rm W}_{j,k}}{2}\cdot\frac{(h_1)^{\rm E}_{j,k}-(h_1)^{\rm W}_{j,k}}{\Delta x},\quad \overline{\mathbf{N}}^{(5)}_{j,k}=-r\cdot\overline{\mathbf{N}}^{(2)}_{j,k},\\
&\overline{\mathbf{N}}^{(3)}_{j,k}=g\frac{(h_1)^{\rm N}_{j,k}+w^{\rm N}_{j,k}+(h_1)^{\rm S}_{j,k}+w^{\rm S}_{j,k}}{2}\cdot\frac{(h_1)^{\rm N}_{j,k}-(h_1)^{\rm S}_{j,k}}{\Delta y},\quad \overline{\mathbf{N}}^{(6)}_{j,k}=-r\cdot\overline{\mathbf{N}}^{(3)}_{j,k}.
\end{aligned}\tag{3.16}$$

3.5. Well-balanced discretization of the geometric source term. The discretization $\overline{\mathbf{S}}_{j,k}$ of the nonzero components of the geometric source term should be such that the resulting central-upwind scheme (3.5) preserves stationary steady-state solutions $\mathbf{U}=(C_1,0,0,C_2,0,0)^T$. As in the 1-D case, the one-sided speeds computed for the steady states satisfy the following relations: $a^{+}_{j+\frac12,k}=-a^{-}_{j+\frac12,k}$ and $b^{+}_{j,k+\frac12}=-b^{-}_{j,k+\frac12}$. Also, we have that the reconstructed point values of $\mathbf{U}$ are

$$\begin{aligned}
&\left((h_1)^{\rm E,W,S,N}_{j,k},(q_1)^{\rm E,W,S,N}_{j,k},(p_1)^{\rm E,W,S,N}_{j,k},w^{\rm E,W,S,N}_{j,k},(q_2)^{\rm E,W,S,N}_{j,k},(p_2)^{\rm E,W,S,N}_{j,k}\right)^T\\
&\qquad=(C_1,0,0,C_2,0,0)^T,
\end{aligned}$$

and, therefore, most of the components of the flux difference terms on the RHS of (3.5) vanish at the steady states:

$$\begin{aligned}
&-\frac{\left(\mathbf{H}^x_{j+\frac12,k}\right)^{(i)}-\left(\mathbf{H}^x_{j-\frac12,k}\right)^{(i)}}{\Delta x}=0,\qquad i=1,2,3,4,6,\\
&-\frac{\left(\mathbf{H}^y_{j,k+\frac12}\right)^{(i)}-\left(\mathbf{H}^y_{j,k-\frac12}\right)^{(i)}}{\Delta y}=0,\qquad i=1,2,3,4,5.
\end{aligned}$$

The only two nonzero flux contributions are

$$\begin{aligned}
&-\frac{\left(\mathbf{H}^x_{j+\frac12,k}\right)^{(5)}-\left(\mathbf{H}^x_{j-\frac12,k}\right)^{(5)}}{\Delta x}=g(C_2+rC_1)\frac{B_{j+\frac12,k}-B_{j-\frac12,k}}{\Delta x},\\
&-\frac{\left(\mathbf{H}^y_{j,k+\frac12}\right)^{(6)}-\left(\mathbf{H}^y_{j,k-\frac12}\right)^{(6)}}{\Delta y}=g(C_2+rC_1)\frac{B_{j,k+\frac12}-B_{j,k-\frac12}}{\Delta y}.
\end{aligned}\tag{3.17}$$

Since for stationary steady states the discretization (3.16) of the nonconservative products results in $\overline{\mathbf{N}}_{j,k}=\mathbf{0}$, stationary steady states will be preserved if (3.17) is

canceled by the contribution of the source term in (3.5). For example, the following discretization of the nonzero components of the source cell averages will achieve the cancellation goal:

$$\begin{aligned}\overline{\mathbf{S}}^{(5)}_{j,k} &\approx -g\frac{\left(w^{\mathrm{E}}_{j,k}+w^{\mathrm{W}}_{j,k}+\left(\widehat{h}_1\right)^{\mathrm{E}}_{j,k}+\left(\widehat{h}_1\right)^{\mathrm{W}}_{j,k}\right)}{2}\cdot\frac{\left(B_{j+\frac12,k}-B_{j-\frac12,k}\right)}{\Delta x},\\ \overline{\mathbf{S}}^{(6)}_{j,k} &\approx -g\frac{\left(w^{\mathrm{N}}_{j,k}+w^{\mathrm{S}}_{j,k}+\left(\widehat{h}_1\right)^{\mathrm{S}}_{j,k}+\left(\widehat{h}_1\right)^{\mathrm{N}}_{j,k}\right)}{2}\cdot\frac{\left(B_{j,k+\frac12}-B_{j,k-\frac12}\right)}{\Delta y}.\end{aligned}\tag{3.18}$$

3.6. Properties of the scheme. The use of the geometric source term discretization (3.18) ensures that the resulting semidiscrete central-upwind scheme (3.5) is well-balanced. Next, we show that it also preserves the positivity of the fluid depths h_1 and h_2 of both layers, namely, that $(\overline{h}_1)^n_{j,k}\ge 0$ and $(\overline{h}_2)^n_{j,k}\ge 0$ for all j,k at all time levels $t=t^n$. More precisely, the following theorem is true.

THEOREM 3.1. *Consider the 2-D two-layer shallow water system* (3.1) *and the central-upwind semidiscrete scheme* (3.5) and (3.7)–(3.18). *Assume that the system of ODEs* (3.5) *is discretized using the forward Euler method and that the cell averages of both layer depths at time $t=t^n$ are nonnegative, that is, $(\overline{h}_1)^n_{j,k}\ge 0$ and $(\overline{h}_2)^n_{j,k}=\overline{w}^n_{j,k}-B_{j,k}\ge 0$ for all (j,k). Then at the next level $t=t^{n+1}$, $(\overline{h}_1)^{n+1}_{j,k}\ge 0$ and $(\overline{h}_2)^{n+1}_{j,k}=\overline{w}^{n+1}_{j,k}-B_{j,k}\ge 0$ for all (j,k), provided $\Delta t\le\min\{\frac{\Delta x}{4a},\frac{\Delta y}{4b}\}$, where a and b are given by $a:=\max_{j,k}\{a^+_{j+\frac12,k},-a^-_{j+\frac12,k}\}$ and $b:=\max_{j,k}\{b^+_{j,k+\frac12},-b^-_{j,k+\frac12}\}$, respectively.*

Proof. The proof of this theorem follows the steps of the proof of Theorem 2.1. We write the first and the fourth components in (3.5) together with the forward Euler temporal discretization as

$$\begin{aligned}(\overline{h}_1)^{n+1}_{j,k}=(\overline{h}_1)^n_{j,k}&-\lambda\left[\left(\mathbf{H}^x_{j+\frac12,k}\right)^{(1)}-\left(\mathbf{H}^x_{j-\frac12,k}\right)^{(1)}\right]\\ &-\mu\left[\left(\mathbf{H}^y_{j,k+\frac12}\right)^{(1)}-\left(\mathbf{H}^y_{j,k-\frac12}\right)^{(1)}\right]\end{aligned}\tag{3.19}$$

and

$$\begin{aligned}\overline{w}^{n+1}_{j,k}=\overline{w}^n_{j,k}&-\lambda\left[\left(\mathbf{H}^x_{j+\frac12,k}\right)^{(4)}-\left(\mathbf{H}^x_{j-\frac12,k}\right)^{(4)}\right]\\ &-\mu\left[\left(\mathbf{H}^y_{j,k+\frac12}\right)^{(4)}-\left(\mathbf{H}^y_{j,k-\frac12}\right)^{(4)}\right],\end{aligned}\tag{3.20}$$

where $\lambda:=\Delta t/\Delta x$, $\mu:=\Delta t/\Delta y$, and the numerical fluxes are evaluated at time level $t=t^n$. Since

$$\left(\mathbf{H}^x_{j+\frac12,k}\right)^{(1)}=\frac{a^+_{j+\frac12,k}(q_1)^{\mathrm{E}}_{j,k}-a^-_{j+\frac12,k}(q_1)^{\mathrm{W}}_{j+1,k}}{a^+_{j+\frac12,k}-a^-_{j+\frac12,k}}+\frac{a^+_{j+\frac12,k}a^-_{j+\frac12,k}}{a^+_{j+\frac12,k}-a^-_{j+\frac12,k}}\left[(h_1)^{\mathrm{W}}_{j+1,k}-(h_1)^{\mathrm{E}}_{j,k}\right]$$

and

$$\left(\mathbf{H}^y_{j,k+\frac12}\right)^{(1)}=\frac{b^+_{j,k+\frac12}(p_1)^{\mathrm{N}}_{j,k}-b^-_{j,k+\frac12}(p_1)^{\mathrm{S}}_{j,k+1}}{b^+_{j,k+\frac12}-b^-_{j,k+\frac12}}+\frac{b^+_{j,k+\frac12}b^-_{j,k+\frac12}}{b^+_{j,k+\frac12}-b^-_{j,k+\frac12}}\left[(h_1)^{\mathrm{S}}_{j,k+1}-(h_1)^{\mathrm{N}}_{j,k}\right],$$

we use (3.15) and the fact that $(\overline{h}_1)^n_{j,k} = ((h_1)^{\rm W}_{j,k} + (h_1)^{\rm E}_{j,k} + (h_1)^{\rm S}_{j,k} + (h_1)^{\rm N}_{j,k})/4$ to obtain

$$
\begin{aligned}
\left(\overline{h}_1\right)^{n+1}_{j,k} = &\left[\frac{1}{4} + \lambda a^-_{j-\frac12,k}\left(\frac{a^+_{j-\frac12,k} - (u_1)^{\rm W}_{j,k}}{a^+_{j-\frac12,k} - a^-_{j-\frac12,k}}\right)\right](h_1)^{\rm W}_{j,k}\\
&+\left[\frac{1}{4} - \lambda a^+_{j+\frac12,k}\left(\frac{(u_1)^{\rm E}_{j,k} - a^-_{j+\frac12,k}}{a^+_{j+\frac12,k} - a^-_{j+\frac12,k}}\right)\right](h_1)^{\rm E}_{j,k}\\
&-\lambda a^-_{j+\frac12,k}\left(\frac{a^+_{j+\frac12,k} - (u_1)^{\rm W}_{j+1,k}}{a^+_{j+\frac12,k} - a^-_{j+\frac12,k}}\right)(h_1)^{\rm W}_{j+1,k}\\
&+\lambda a^+_{j-\frac12,k}\left(\frac{(u_1)^{\rm E}_{j-1,k} - a^-_{j-\frac12,k}}{a^+_{j-\frac12,k} - a^-_{j-\frac12,k}}\right)(h_1)^{\rm E}_{j-1,k}\\
&+\left[\frac{1}{4} + \mu b^-_{j,k-\frac12}\left(\frac{b^+_{j,k-\frac12} - (v_1)^{\rm S}_{j,k}}{b^+_{j,k-\frac12} - b^-_{j,k-\frac12}}\right)\right](h_1)^{\rm S}_{j,k}\\
&+\left[\frac{1}{4} - \mu b^+_{j,k+\frac12}\left(\frac{(v_1)^{\rm N}_{j,k} - b^-_{j,k+\frac12}}{b^+_{j,k+\frac12} - b^-_{j,k+\frac12}}\right)\right](h_1)^{\rm N}_{j,k}\\
&-\mu b^-_{j,k+\frac12}\left(\frac{b^+_{j,k+\frac12} - (v_1)^{\rm S}_{j,k+1}}{b^+_{j,k+\frac12} - b^-_{j,k+\frac12}}\right)(h_1)^{\rm S}_{j,k+1}\\
&+\mu b^+_{j,k-\frac12}\left(\frac{(v_1)^{\rm N}_{j,k-1} - b^-_{j,k-\frac12}}{b^+_{j,k-\frac12} - b^-_{j,k-\frac12}}\right)(h_1)^{\rm N}_{j,k-1}.
\end{aligned}
\tag{3.21}
$$

The use of the positivity preserving reconstruction $\widetilde{h}_1$ ensures that $(h_1)^{\rm E,W,S,N}_{j,k} \geq 0$ for all j,k. Also, the local speeds of propagation, defined at the end of section 3.3, satisfy the inequalities $a^+_{j\pm\frac12,k} \geq 0$, $a^-_{j\pm\frac12,k} \leq 0$, $b^+_{j,k\pm\frac12} \geq 0$, $b^-_{j,k\pm\frac12} \leq 0$, and

$$
\begin{aligned}
&0 \leq \frac{a^+_{j-\frac12,k} - (u_1)^{\rm W}_{j,k}}{a^+_{j-\frac12,k} - a^-_{j-\frac12,k}} \leq 1, \qquad 0 \leq \frac{(u_1)^{\rm E}_{j,k} - a^-_{j+\frac12,k}}{a^+_{j+\frac12,k} - a^-_{j+\frac12,k}} \leq 1,\\
&0 \leq \frac{b^+_{j,k-\frac12} - (v_1)^{\rm S}_{j,k}}{b^+_{j,k-\frac12} - b^-_{j,k-\frac12}} \leq 1, \qquad 0 \leq \frac{(v_1)^{\rm N}_{j,k} - b^-_{j,k+\frac12}}{b^+_{j,k+\frac12} - b^-_{j,k+\frac12}} \leq 1
\end{aligned}
$$

for all j,k. Therefore, all terms in the second and the fourth row of the RHS of (3.21) are nonnegative. The terms in the first and the third rows there are also nonnegative under the assumed CFL restrictions $\lambda a \leq 1/4$ and $\mu b \leq 1/4$, where $a := \max_{j,k}\{a^+_{j+\frac12,k}, -a^-_{j+\frac12,k}\}$ and $b := \max_{j,k}\{b^+_{j,k+\frac12}, -b^-_{j,k+\frac12}\}$.

Next, we show that the cell averages of the second layer depth $\{(\overline{h}_2)^{n+1}_{j,k}\}$ are also nonnegative. Using (3.9), we obtain

$$
\left(\mathbf{H}^x_{j+\frac12,k}\right)^{(4)} = \frac{a^+_{j+\frac12,k}(q_2)^{\rm E}_{j,k} - a^-_{j+\frac12,k}(q_2)^{\rm W}_{j+1,k}}{a^+_{j+\frac12,k} - a^-_{j+\frac12,k}} + \frac{a^+_{j+\frac12,k}a^-_{j+\frac12,k}}{a^+_{j+\frac12,k} - a^-_{j+\frac12,k}}\left[w^{\rm W}_{j+1,k} - w^{\rm E}_{j,k}\right]
$$

$$= \frac{a^+_{j+\frac12,k}(q_2)^{\mathrm{E}}_{j,k} - a^-_{j+\frac12,k}(q_2)^{\mathrm{W}}_{j+1,k}}{a^+_{j+\frac12,k} - a^-_{j+\frac12,k}} + \frac{a^+_{j+\frac12,k}a^-_{j+\frac12,k}}{a^+_{j+\frac12,k} - a^-_{j+\frac12,k}}\left[(h_2)^{\mathrm{W}}_{j+1,k} - (h_2)^{\mathrm{E}}_{j,k}\right] \tag{3.22}$$

and

$$\begin{aligned}\left(\mathbf{H}^y_{j,k+\frac12}\right)^{(4)} &= \frac{b^+_{j,k+\frac12}(p_2)^{\mathrm{N}}_{j,k} - b^-_{j,k+\frac12}(p_2)^{\mathrm{S}}_{j,k+1}}{b^+_{j,k+\frac12} - b^-_{j,k+\frac12}} + \frac{b^+_{j,k+\frac12}b^-_{j,k+\frac12}}{b^+_{j,k+\frac12} - b^-_{j,k+\frac12}}\left[w^{\mathrm{S}}_{j,k+1} - w^{\mathrm{N}}_{j,k}\right]\\ &= \frac{b^+_{j,k+\frac12}(p_2)^{\mathrm{N}}_{j,k} - b^-_{j,k+\frac12}(p_2)^{\mathrm{S}}_{j,k+1}}{b^+_{j,k+\frac12} - b^-_{j,k+\frac12}} + \frac{b^+_{j,k+\frac12}b^-_{j,k+\frac12}}{b^+_{j,k+\frac12} - b^-_{j,k+\frac12}}\left[(h_2)^{\mathrm{S}}_{j,k+1} - (h_2)^{\mathrm{N}}_{j,k}\right].\end{aligned} \tag{3.23}$$

It follows from (3.4) that

$$\begin{aligned}\overline{w}^n_{j,k} - B_{j,k} &= \frac14\left(w^{\mathrm{E}}_{j,k} + w^{\mathrm{W}}_{j,k} + w^{\mathrm{S}}_{j,k} + w^{\mathrm{N}}_{j,k}\right)\\ &\quad - \frac14\left(B_{j+\frac12,k} + B_{j-\frac12,k} + B_{j,k+\frac12} + B_{j,k-\frac12}\right)\\ &= \frac14\left((h_2)^{\mathrm{E}}_{j,k} + (h_2)^{\mathrm{W}}_{j,k} + (h_2)^{\mathrm{S}}_{j,k} + (h_2)^{\mathrm{N}}_{j,k}\right),\end{aligned}$$

and, thus, subtracting $B_{j,k}$ from both sides of (3.20), using (3.22), (3.23), and (3.15), and rearranging the terms, we arrive at

$$\begin{aligned}(\overline{h}_2)^{n+1}_{j,k} = &\left[\frac14 + \lambda a^-_{j-\frac12,k}\left(\frac{a^+_{j-\frac12,k} - (u_2)^{\mathrm{W}}_{j,k}}{a^+_{j-\frac12,k} - a^-_{j-\frac12,k}}\right)\right](h_2)^{\mathrm{W}}_{j,k}\\ &+ \left[\frac14 - \lambda a^+_{j+\frac12,k}\left(\frac{(u_2)^{\mathrm{E}}_{j,k} - a^-_{j+\frac12,k}}{a^+_{j+\frac12,k} - a^-_{j+\frac12,k}}\right)\right](h_2)^{\mathrm{E}}_{j,k}\\ &- \lambda a^-_{j+\frac12,k}\left(\frac{a^+_{j+\frac12,k} - (u_2)^{\mathrm{W}}_{j+1,k}}{a^+_{j+\frac12,k} - a^-_{j+\frac12,k}}\right)(h_2)^{\mathrm{W}}_{j+1,k}\\ &+ \lambda a^+_{j-\frac12,k}\left(\frac{(u_2)^{\mathrm{E}}_{j-1,k} - a^-_{j-\frac12,k}}{a^+_{j-\frac12,k} - a^-_{j-\frac12,k}}\right)(h_2)^{\mathrm{E}}_{j-1,k}\\ &+ \left[\frac14 + \mu b^-_{j,k-\frac12}\left(\frac{b^+_{j,k-\frac12} - (v_2)^{\mathrm{S}}_{j,k}}{b^+_{j,k-\frac12} - b^-_{j,k-\frac12}}\right)\right](h_2)^{\mathrm{S}}_{j,k}\\ &+ \left[\frac14 - \mu b^+_{j,k+\frac12}\left(\frac{(v_2)^{\mathrm{N}}_{j,k} - b^-_{j,k+\frac12}}{b^+_{j,k+\frac12} - b^-_{j,k+\frac12}}\right)\right](h_2)^{\mathrm{N}}_{j,k}\\ &- \mu b^-_{j,k+\frac12}\left(\frac{b^+_{j,k+\frac12} - (v_2)^{\mathrm{S}}_{j,k+1}}{b^+_{j,k+\frac12} - b^-_{j,k+\frac12}}\right)(h_2)^{\mathrm{S}}_{j,k+1}\\ &+ \mu b^+_{j,k-\frac12}\left(\frac{(v_2)^{\mathrm{N}}_{j,k-1} - b^-_{j,k-\frac12}}{b^+_{j,k-\frac12} - b^-_{j,k-\frac12}}\right)(h_2)^{\mathrm{N}}_{j,k-1}.\end{aligned} \tag{3.24}$$

Next, we argue as in the case for $(\overline{h}_1)^{n+1}_{j,k}$ to show that all eight terms on the RHS of (3.24) are nonnegative. The correction procedure (3.10)–(3.13) for the reconstruction $\widetilde{w}$ guarantees that the computed point values $(h_2)^{\mathrm{E,W,S,N}}_{j,k} \geq 0$ for all j,k. It follows from the definition of the local speeds, given at the end of section 3.3, that

$$0 \leq \frac{a^+_{j-\frac{1}{2},k} - (u_2)^{\mathrm{W}}_{j,k}}{a^+_{j-\frac{1}{2},k} - a^-_{j-\frac{1}{2},k}} \leq 1, \qquad 0 \leq \frac{(u_2)^{\mathrm{E}}_{j,k} - a^-_{j+\frac{1}{2},k}}{a^+_{j+\frac{1}{2},k} - a^-_{j+\frac{1}{2},k}} \leq 1,$$

$$0 \leq \frac{b^+_{j,k-\frac{1}{2}} - (v_2)^{\mathrm{S}}_{j,k}}{b^+_{j,k-\frac{1}{2}} - b^-_{j,k-\frac{1}{2}}} \leq 1, \qquad 0 \leq \frac{(v_2)^{\mathrm{N}}_{j,k} - b^-_{j,k+\frac{1}{2}}}{b^+_{j,k+\frac{1}{2}} - b^-_{j,k+\frac{1}{2}}} \leq 1,$$

which, together with the CFL restrictions $\lambda a \leq 1/4$ and $\mu b \leq 1/4$, ensures that all terms on the RHS of (3.24) are nonnegative. This completes the proof. □

Remark 3.1. Theorem 3.1 is still valid if one uses a higher-order SSP ODE solver (either the Runge–Kutta or the multistep one), because such solvers can be written as a convex combination of several forward Euler steps.

3.7. Numerical experiments. We now demonstrate the performance of our 2-D scheme on two numerical examples. In both of them, the flow stays in the hyperbolic regime so the one-sided local speeds can be computed using the first-order approximation of the eigenvalues. The parameters θ_1 and θ_2 in the calculation of the numerical derivatives in (3.8) are tuned to the most diffusive regime ($\theta_1 = \theta_2 = 1$) in order to minimize spurious oscillations. In both sections 3.7.1 and 3.7.2, the gravitational constant is $g = 10$ and the density ratio is $r = 0.98$.

3.7.1. Interface propagation. In this example, which is a 2-D extension of the 1-D example studied in section 2.7.3, a round-shape interface propagates in the northeast direction. The initial data are

$$(h_1, q_1, p_1, h_2, q_2, p_2)(x, y, 0) = \begin{cases} (0.50, 1.250, 1.250, 0.50, 1.250, 1.250) & (x,y) \in \Omega, \\ (0.45, 1.125, 1.125, 0.55, 1.375, 1.375) & \text{otherwise}, \end{cases}$$

where

$$\Omega = \{x < -0.5, y < 0\} \cup \{(x+0.5)^2 + (y+0.5)^2 < 0.25\} \cup \{x < 0, y < -0.5\}. \tag{3.25}$$

The initial location of the interface ($\partial\Omega$) is shown by the dashed line in the contour plots of h_1 in the right column of Figure 3.1. The bottom in this example is flat ($B(x,y) \equiv -1$).

We compute the solution of this initial value problem at time $t = 0.1$ on a sequence of uniform grids with $\Delta x = \Delta y = 1/200$, $1/400$, and $1/800$. The results (ε and h_1) are shown in Figure 3.1. Even though this problem is genuinely 2-D, its solution

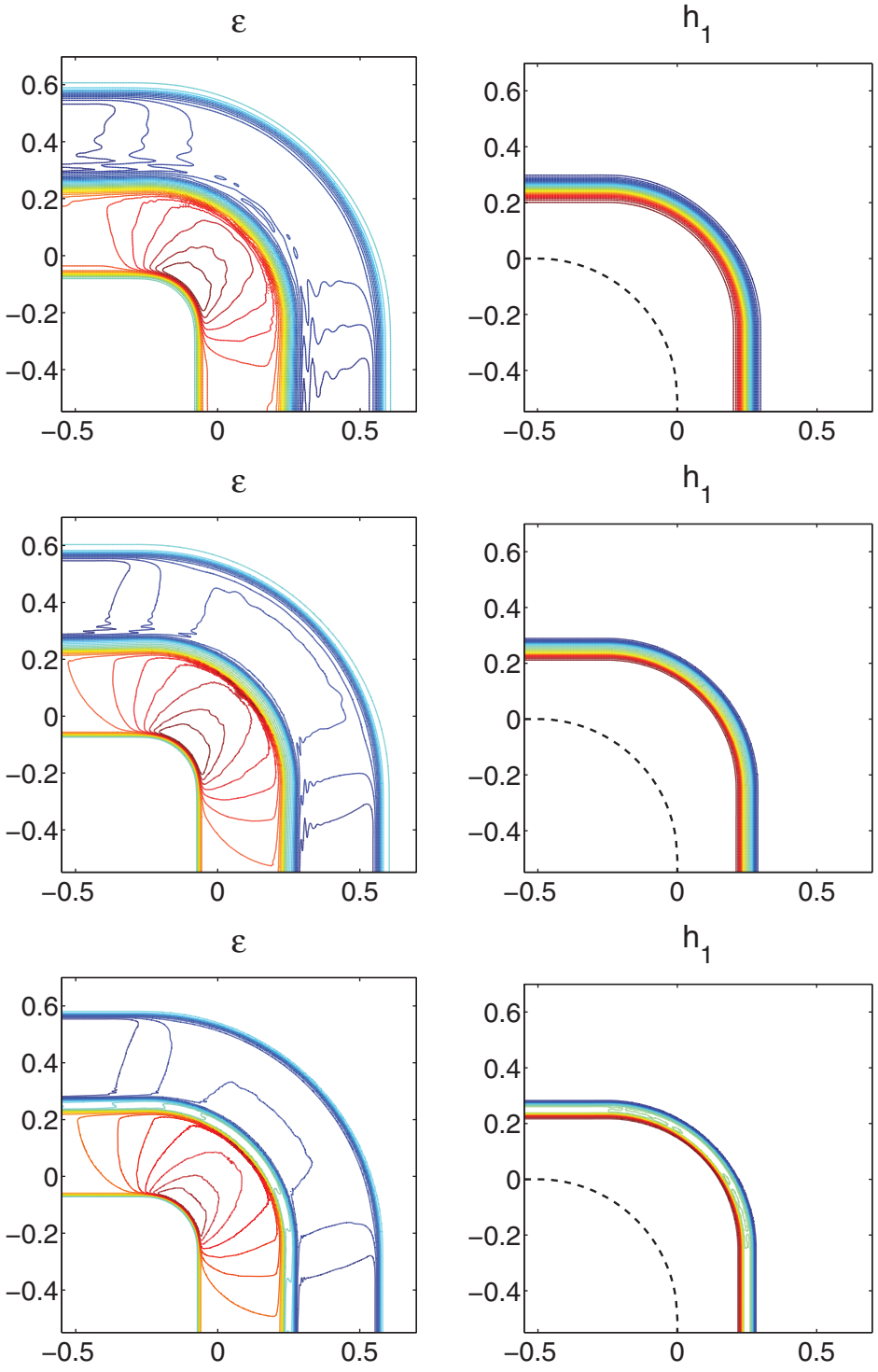

FIG. 3.1. *2-D interface propagation problem: water surface ε and h_1-component of the solution computed on three uniform grids with $\Delta x = \Delta y = 1/200$ (upper row), $1/400$ (middle row), and $1/800$ (lower row). The dashed line represents the initial interface location.*

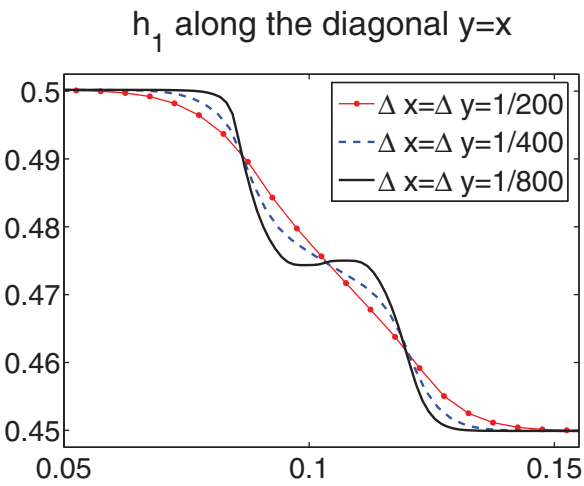

FIG. 3.2. 2-*D interface propagation problem: a diagonal slice of* h_1*, zoom at the interface area.*

structure is similar to the solution of the original 1-D interface propagation problem from section 2.7.3: 4 waves are developed and propagated with 4 different characteristic speeds along the dominant diagonal $y = x$. As in the 1-D case, an intermediate state emerges. This may be clearly seen in Figure 3.2, where we plot the diagonal slice of h_1.

As one may notice, the low resolution solution (Figure 3.1 (upper row)) contains some small oscillations (they are indeed small since the magnitude of ε is small by itself in this example), which seem to disappear as the mesh is refined.

3.7.2. Propagation of the interface over a nonflat bottom. We now extend the previous example to the case of a nonflat bottom topography. We take the Gaussian-shaped bottom function

$$B(x,y) = 0.05e^{-100\left(x^2+y^2\right)} - 1$$

and the following initial data:

$$(h_1,u_1,v_1,w,u_2,v_2)(x,y,0) = \begin{cases} (0.50,2.5,2.5,-0.50,2.5,2.5) & (x,y)\in\Omega, \\ (0.45,2.5,2.5,-0.45,2.5,2.5) & \text{otherwise}, \end{cases}$$

where Ω is given by (3.25).

We compute the solution of this initial value problem at time $t = 0.1$ on a sequence of uniform grids with $\Delta x = \Delta y = 1/200$, $1/400$, and $1/800$ and present the obtained results (ε and h_1) in Figure 3.3. Due to a nonflat bottom topography, the solution of this problem develops a very complicated wave structure. The obtained numerical solution seems to be convergent. One can observe some small oscillations in the h_1-component. We believe that this happens since the surface waves are not so small in this example (see the left column of Figure 3.3), and, thus, the influence of the nonconservative product terms is not negligibly small.

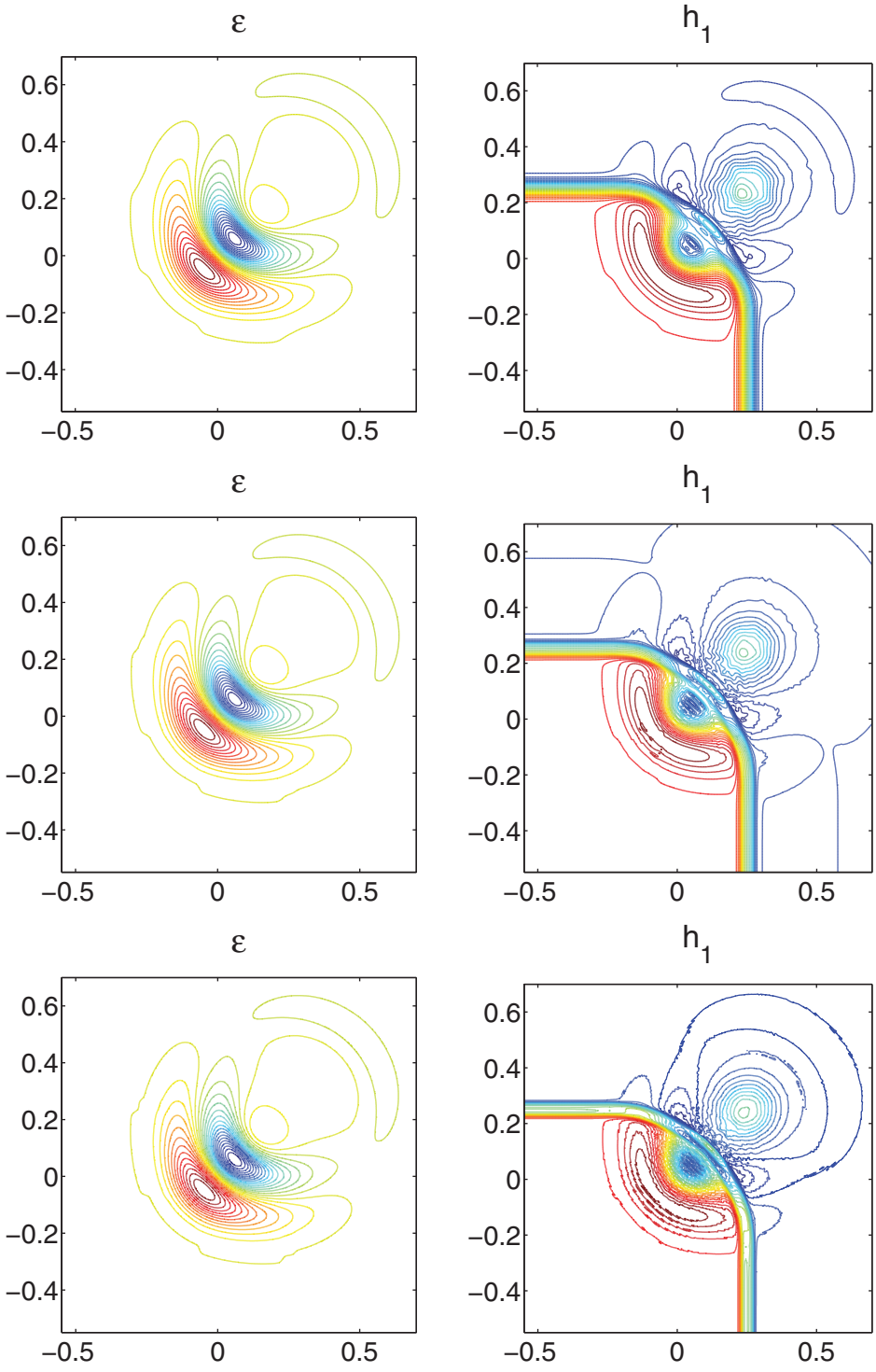

FIG. 3.3. *Propagation of the interface over a nonflat bottom: water surface* ε *(30 contour lines uniformly distributed between* $\min \varepsilon \approx -0.0066$ *and* $\max \varepsilon \approx 0.0072$*) and* h_1 *computed on three uniform grids with* $\Delta x = \Delta y = 1/200$ *(upper row),* $1/400$ *(middle row), and* $1/800$ *(lower row).*

REFERENCES

[1] R. Abgrall and S. Karni, *Two-layer shallow water systems: A relaxation approach*, SIAM J. Sci. Comput., to appear.

[2] E. Audusse, *A multilayer Saint-Venant model: Derivation and numerical validation*, Discrete Contin. Dyn. Syst. Ser. B, 5 (2005), pp. 189–214.

[3] F. Berger and J.-F. Colombeau, *Numerical solutions of one-pressure models in multifluid flows*, SIAM J. Numer. Anal., 32 (1995), pp. 1139–1154.

[4] F. Bouchut and T. Morales de Luna, *An entropy satisfying scheme for two-layer shallow water equations with uncoupled treatment*, M2AN Math. Model. Numer. Anal., 42 (2008), pp. 683–698.

[5] M. Castro, J. Macías, and C. Parés, *A Q-scheme for a class of systems of coupled conservation laws with source term. Application to a two-layer 1-D shallow water system*, M2AN Math. Model. Numer. Anal., 35 (2001), pp. 107–127.

[6] M.J. Castro, J. Macías, C. Parés, J.A. García-Rodríguez, and E. Vázquez-Cendón, *A two-layer finite volume model for flows through channels with irregular geometry: Computation of maximal exchange solutions. Application to the Strait of Gibraltar*, Commun. Nonlinear Sci. Numer. Simul., 9 (2004), pp. 241–249.

[7] J.-J. Cauret, J.-F. Colombeau, and A.Y. LeRoux, *Discontinuous generalized solutions of nonlinear nonconservative hyperbolic equations*, J. Math. Anal. Appl., 139 (1989), pp. 552–573.

[8] J.F. Colombeau, A. Heibig, and M. Oberguggenberger, *Generalized solutions to partial differential equations of evolution type*, Acta Appl. Math., 45 (1996), pp. 115–142.

[9] J.-F. Colombeau, *Multiplication of Distributions: A Tool in Mathematics, Numerical Engineering and Theoretical Physics*, Lecture Notes in Math. 1532, Springer-Verlag, Berlin, 1992.

[10] G. Dal Maso, P.G. Lefloch, and F. Murat, *Definition and weak stability of nonconservative products*, J. Math. Pures Appl., 74 (1995), pp. 483–548.

[11] A.J.C. de Saint-Venant, *Thèorie du mouvement non-permanent des eaux, avec application aux crues des rivière at à l'introduction des marèes dans leur lit.*, C.R. Acad. Sci. Paris, 73 (1871), pp. 147–154.

[12] M.J. Castro Díaz, T. Chacón Rebollo, E.D. Fernández-Nieto, and C. Parés, *On well-balanced finite volume methods for nonconservative nonhomogeneous hyperbolic systems*, SIAM J. Sci. Comput., 29 (2007), pp. 1093–1126.

[13] B. Einfeldt, *On Godunov-type methods for gas dynamics*, SIAM J. Numer. Anal., 25 (1988), pp. 294–318.

[14] D. Farmer and L. Armi, *Maximal two-layer exchange over a sill and through a combination of a sill and contraction with barotropic flow*, J. Fluid Mech., 164 (1986), pp. 53–76.

[15] E. Godlewski and P.-A. Raviart, *Numerical Approximation of Hyperbolic Systems of Conservation Laws*, Appl. Math. Sci. 118, Springer-Verlag, New York, 1996.

[16] S. Gottlieb, C.-W. Shu, and E. Tadmor, *Strong stability-preserving high-order time discretization methods*, SIAM Rev., 43 (2001), pp. 89–112.

[17] A. Harten, P. D. Lax, and B. van Leer, *On upstream differencing and Godunov-type schemes for hyperbolic conservation laws*, SIAM Rev., 25 (1983), pp. 35–61.

[18] D. Kröner, *Numerical Schemes for Conservation Laws*, Adv. Numer. Math., John Wiley & Sons, Chichester, 1997.

[19] A. Kurganov and D. Levy, *Central-upwind schemes for the Saint-Venant system*, M2AN Math. Model. Numer. Anal., 36 (2002), pp. 397–425.

[20] A. Kurganov and C.-T. Lin, *On the reduction of numerical dissipation in central-upwind schemes*, Commun. Comput. Phys., 2 (2007), pp. 141–163.

[21] A. Kurganov, S. Noelle, and G. Petrova, *Semidiscrete central-upwind schemes for hyperbolic conservation laws and Hamilton–Jacobi equations*, SIAM J. Sci. Comput., 23 (2001), pp. 707–740.

[22] A. Kurganov and G. Petrova, *A second-order well-balanced positivity preserving central-upwind scheme for the Saint-Venant system*, Commun. Math. Sci., 5 (2007), pp. 133–160.

[23] A. Kurganov and E. Tadmor, *New high resolution central schemes for nonlinear conservation laws and convection-diffusion equations*, J. Comput. Phys., 160 (2000), pp. 241–282.

[24] A. Kurganov and E. Tadmor, *Solution of two-dimensional Riemann problems for gas dynamics without Riemann problem solvers*, Numer. Methods Partial Differential Equations, 18 (2002), pp. 584–608.

[25] P.G. LeFloch, *Graph solutions of nonlinear hyperbolic systems*, J. Hyperbolic Differ. Equ., 1 (2004), pp. 643–689.

[26] R.J. LeVeque, *Finite Volume Methods for Hyperbolic Problems*, Cambridge Texts Appl. Math., Cambridge University Press, Cambridge, 2002.

[27] K.-A. Lie and S. Noelle, *On the artificial compression method for second-order nonoscillatory central difference schemes for systems of conservation laws*, SIAM J. Sci. Comput., 24 (2003), pp. 1157–1174.

[28] J. Macías, C. Pares, and M.J. Castro, *Improvement and generalization of a finite element shallow-water solver to multi-layer systems*, Internat. J. Numer. Methods Fluids, 31 (1999), pp. 1037–1059.

[29] M. Mignotte and D. Stefanescu, *On an Estimation of Polynomial Roots by Lagrange*, Technical report 025/2002, IRMA, Strasbourg, 2002; also available online from http://hal.archives-ouvertes.fr/hal-00129675/en/.

[30] H. Nessyahu and E. Tadmor, *Nonoscillatory central differencing for hyperbolic conservation laws*, J. Comput. Phys., 87 (1990), pp. 408–463.

[31] C. Parés and M. Castro, *On the well-balance property of Roe's method for nonconservative hyperbolic systems. Applications to shallow-water systems*, M2AN Math. Model. Numer. Anal., 38 (2004), pp. 821–852.

[32] J.B. Schijf and J.C. Schonfeld, *Theoretical considerations on the motion of salt and fresh water*, in Proceedings of the Minnesota International Hydraulics Conv., Minneapolis, MN, American Society of Civil Engineers, 1953, pp. 321–333.

[33] C.-W. Shu, *Total-variation-diminishing time discretizations*, SIAM J. Sci. Stat. Comput., 9 (1988), pp. 1073–1084.

[34] C.-W. Shu and S. Osher, *Efficient implementation of essentially non-oscillatory shock-capturing schemes*, J. Comput. Phys., 77 (1988), pp. 439–471.

[35] P.K. Sweby, *High resolution schemes using flux limiters for hyperbolic conservation laws*, SIAM J. Numer. Anal., 21 (1984), pp. 995–1011.

[36] B. van Leer, *Towards the ultimate conservative difference scheme.* V. *A second-order sequel to Godunov's method*, J. Comput. Phys., 32 (1979), pp. 101–136.

[37] Y. Xing and C.-W. Shu, *High order finite difference WENO schemes with the exact conservation property for the shallow water equations*, J. Comput. Phys., 208 (2005), pp. 206–227.